KMS Technologies – KJT Enterprises Inc.

Chapter 4
Data Interpretation

extract from

Strack, K.-M., 1992**,** reprinted 1999
Exploration with deep transient electromagnetic: Elsevier, 373 pp.

Chapter 4
Data Interpretation

There are several different ways to interpret EM field data. One way is to normalize the data and to generate anomaly maps. When TEM is applied in the mining industry the results are usually displayed on parallel profiles and maps because in most cases multi-dimensional anomalies are being considered. Another way is a quantitative interpretation to obtain an earth model with resistivities and layer thicknesses. This is usually called inversion and is the way most EM sounding data is interpreted. Inversion techniques as used for LOTEM data will be discussed. An excellent review of inversion methods can be found in Lines and Treitel (1984). After the initial review of the theoretical concepts, the inversion statistics and newer applications of the inversion such as *profile inversion* and *Occam inversion* are explained using real data examples in this chapter.

Three-dimensional structures are generally very difficult to interpret. One must first use some characteristic effects in the data, such as reversals, to obtain an estimate on how to approach the interpretation problem. This is essential because 3-D modeling algorithms still take a lot of computer time. Different 3-D algorithms can be used for different effects in the data. This allows the derivation of a first quantitative interpretation of the data. After discussing the interpretation of reversals, some selected 3-D models are shown.

ONE-DIMENSIONAL INVERSION

The overall goal of the inversion is to find the optimum earth model which fits the field data using a minimum of computer time. At the same time, it is important to obtain reliability estimates of the inversion run and the resulting model. These inversion statistics allow us to evaluate the result and find the optimum solution. In other scientific disciplines this procedure is called differently: the statisticians talk about *regression*, the electrical engineers talk about *system identification*. The geophysicists talk about *inversion* for two different reasons:

- We are trying to go from the data to the model parameters. This is the inverse way of forward modeling.
- An ill-conditioned matrix is to be inverted, which is a difficult task.

Figures 4.1a and b show the relationship between forward modeling and inversion for

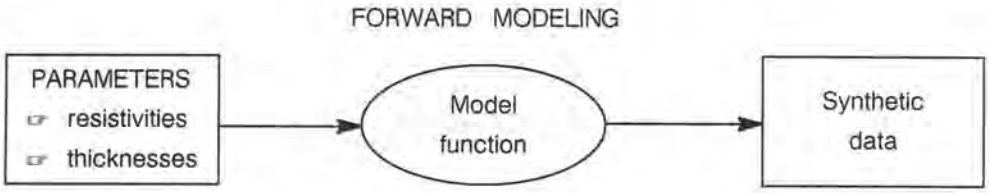

Fig.4.1a: FORWARD modeling functional diagram.

electromagnetic data. In the forward modeling sense we start with the estimated or known geoelectric *model parameters* and calculate the response function or *synthetic data* of our method using a predefined *model function*. The better we can get an idea about our earth model using well logs, other geophysical results and geology, the better our synthetic data will be. In the inverse modeling sense, we use an initial guess to compare our field data with our preconceived model. The more information we can get about our model, the faster we will obtain a reliable result. This additional information is called *a priori* information and can either be incorporated in the initial model or in adjustments of the iteration model. Latter is done in such a way that the known information is maintained and the unknown information is varied to find the optimum solution. In one sentence one could say:

The objective of inversion is to aid the interpreter in such a way that his subjective guess is quantified and thus might appear more objective.

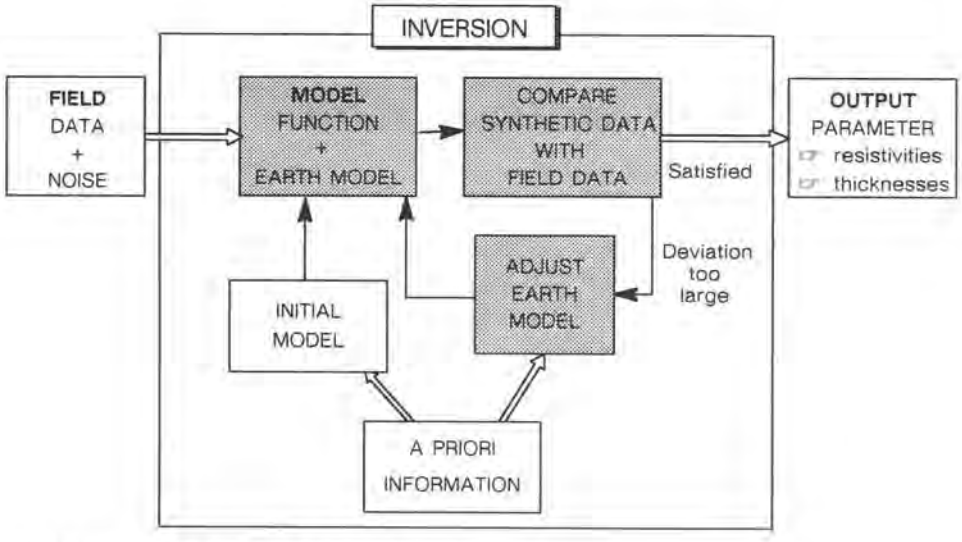

Fig. 4.1b: INVERSE modeling functional diagram.

If we want to calculate the response of an earth model, we must first have all the necessary model parameters available. For electromagnetic methods these are the resistivities ρ_j (j = 1...M) and the thicknesses h_j of the layers (j = 1,...M–1). These parameters describe the model sketched in figure 4.2. We also have a model function telling us how to calculate synthetic data from the model parameters. Let this model function be f or f_i, if evaluated for the i–th synthetic data point (i = 1,...n):

p_j are m parameters, $\rho_1, \ldots \rho_M, h_1, \ldots h_{M-1}$, m= 2 M – 1

$f_i = f_i(\mathbf{p})$ are n model functions,

y_i are the data points measured in the field, or

$y_i = f_i(\mathbf{p})$ are the synthetic data forward modeling case, and

σ_i are the standard deviations of the data points derived from the measurements.

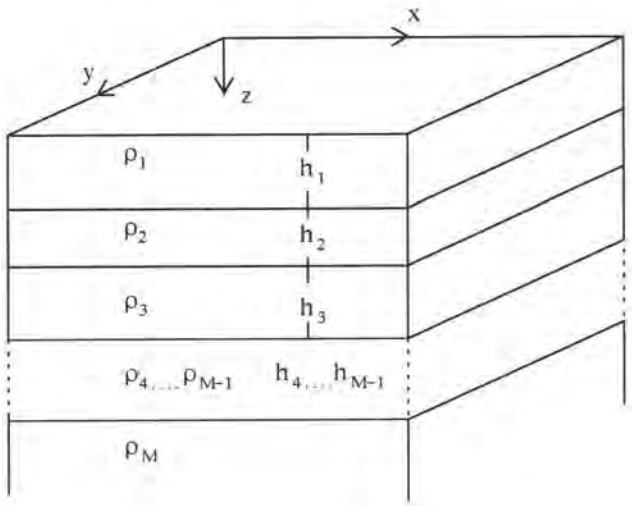

Fig.4.2: Model of a horizontally layered earth made up of M layers with respective resistivities and thicknesses.

All of the above are components of the respective vectors **p**, **f**, **y**, and σ. The forward model curve or synthetic curve is a set of all function values f_i. If you go from the forward modeling to the inverse modeling or inversion, y_i becomes the observed data and f_i the modeled data. This leads us to two main goals of inversion:

- Minimize the difference **q** between the *observed* and *modeled* data:

$$\mathbf{q} = |\mathbf{y} - \mathbf{f}|^2. \tag{4.1}$$

- Estimate the reliability of your model by calculating confidence bounds.

In this chapter, we shall focus on answering the question on how to reach the above two goals for the LOTEM method. More detailed information can be found in Jupp and Vozoff (1975), Vozoff and Jupp (1975), Lines and Treitel (1984), Petry (1987) and Hördt (1989).

Since all parameters are physical parameters and cannot become negative, the inversion is done with logarithmic data and logarithmic parameters. This is also more reasonable from the physical point of view, since electromagnetic waves are damped exponentially in the subsurface (skin effect). It also allows the use of a larger dynamic range in the signal and stabilizes the inversion process.

In a least squares sense, a measure of the error between real data and modeled data is defined by Jackson (1972):

$$\chi^2 = \frac{1}{n} \sum_{i=1}^{n} \frac{(f_i - y_i)^2}{\sigma_i^2}, \tag{4.2}$$

which is the average quadratic deviation between calculated and measured data weighting every data point with its standard deviation. This means that ideally this value is equal to 1, when the the obtained deviation $(f_i - y_i)$ is equal to the expected deviation σ_i.

Deviations larger than 1 from this can have two causes:

- The earth model does not sufficiently describe the real earth. This means a layer-cake description of the earth is not adequate and a multi-dimensional models must be used.
- The calculation of σ_i does not adequately consider all possible sources of error or the error propagation is incorrect.

The latter is the more likely cause (in sedimentary areas), since the standard deviation is derived from the stacking and processing or system errors before stacking do not get considered.

When χ^2 becomes smaller than 1, it means that the problem is underdetermined, i.e. there are more model parameters used than necessary. In this case, it is easily noticed that the data is being overinterpreted and that one is interpreting the noise.

The most common way to minimize the least squares sum is the Gauss-Newton method. This method always works when the problem is linear. For non-linear problems, one first has to linearize the problem by expanding it into a Taylor series:

$$f_i = f_i(\mathbf{p}) \approx f_i(\mathbf{p}_0) + \underbrace{\sum_{j=1}^{m} \left.\frac{\delta f_i(\mathbf{p})}{\delta p_j}\right|_{\mathbf{p}=\mathbf{p}_0} (p_j - p_{j,0})}_{\Delta p_j} \qquad (4.3)$$

or

$$\mathbf{f}(\mathbf{p}) \approx \mathbf{f}(\mathbf{p}_0) + \mathbf{J}\Delta\mathbf{p} = \begin{pmatrix} \frac{\delta f_1}{\delta p_1} & \cdots & \frac{\delta f_m}{\delta p_m} \\ \vdots & & \vdots \\ \frac{\delta f_n}{\delta p_1} & \cdots & \frac{\delta f_n}{\delta p_m} \end{pmatrix} \Delta\mathbf{p} + \mathbf{f}(\mathbf{p}_0)$$

or

$$J_{ij} = \left.\frac{\delta f_i}{\delta p_j}\right|_{\mathbf{p}=\mathbf{p}_0} \qquad i=1, \ldots, n;\ j=1, \ldots, m$$

$$\mathbf{f}(\mathbf{p}) \approx \mathbf{f}(\mathbf{p}_0) + \mathbf{J}\Delta\mathbf{p} \qquad (4.4)$$

J is the Jacobian matrix containing for each data point the derivative of the model functions with respect to the parameters. $\Delta\mathbf{p}$ is the parameter difference vector also sometimes called $\Delta\mathbf{p}$, and $\mathbf{p}_0$ contains the initial guess model parameters. The Jacobian shows how the model function reacts to small changes in the model parameters and can thus be used for sensitivity analysis.

We recall the goal to find the parameter vector **p** such that

$$q = \left| \mathbf{y} - \mathbf{f} \right|^2 = \mathbf{e}^T\mathbf{e} = \text{minimum} \qquad (4.5)$$

where

$\mathbf{e} = \mathbf{y} - \mathbf{f}(\mathbf{p}_0) - \mathbf{J}\Delta\mathbf{p}$ is the difference or error vector.

This error vector can be directly related to the standard deviations of the data and the χ^2 error measure. The inverse standard deviations are written on the main diagonal of the weighting matrix **W** (Jackson, 1972):

$$W_{ij} = \delta_{ij} \frac{1}{\sigma_i} \quad .$$

where $\delta_{ij} = \begin{cases} 1 \text{ for } i=j \\ 0 \text{ otherwise} \end{cases}$ is the Kronecker symbol. Then χ^2 can be written as

$$\chi^2 = \frac{1}{n} \mathbf{e}^T \mathbf{W}^2 \mathbf{e} \tag{4.6}$$

If we define a discrepancy vector

$$\mathbf{g} = \mathbf{y} - \mathbf{f}(\mathbf{p}_0) \qquad \text{then} \qquad \mathbf{e} = \mathbf{g} - \mathbf{J}\Delta\mathbf{p} \text{ and} \tag{4.7}$$

$$\chi^2 = \frac{1}{n} (\mathbf{g} - \mathbf{J}\Delta\mathbf{p})^T \mathbf{W}^2 (\mathbf{g} - \mathbf{J}\Delta\mathbf{p}) \tag{4.8}$$

we must find the minimum of χ^2 which means

$$\frac{\delta \chi^2}{\delta p_j} = 0 \qquad \text{for } j = 1, \ldots m. \tag{4.9}$$

Doing this yields the linear system (Lines and Treitel, 1984):

$$\mathbf{J}^T \mathbf{W}^2 \mathbf{J}\Delta\mathbf{p} = \mathbf{J}^T \mathbf{W}^2 \mathbf{g} \qquad \text{with the solution} \tag{4.10}$$

$$\Delta\mathbf{p} = (\mathbf{J}^T \mathbf{W}^2 \mathbf{J})^{-1} \mathbf{J}^T \mathbf{W}^2 \mathbf{g}, \tag{4.11}$$

If the model function $\mathbf{f}(\mathbf{p})$ is linear, equation 4.4 gives an exact equality. The required parameter vector can be obtained from $\mathbf{p}_1 = \mathbf{p}_0 + \Delta\mathbf{p}$, which is already the solution in a linear case. χ^2 will exhibit a minimum at $\mathbf{p}_1$. For linear cases only, one iteration will yield the solution. For non-linear cases the new obtained parameter vector, $\mathbf{p}_1$, is substituted in the above equation instead of $\mathbf{p}_0$ and the procedure is repeated until convergence is reached.

Figure 4.3 illustrates the above situation. The dashed line represents the error due to the linearization at the parameter $\mathbf{p}_n^{est}$. It is a hyperbola parallel to E at the point $\mathbf{p}_n^{est}$. The next iteration will go to the $\mathbf{p}_{n+1}$ position. There the error is calculated and a similar procedure done until the global minimum has been reached. In doing so, there arise three new questions:

- How do we make sure we always reach the best minimum (which in most cases is the global minimum but sometimes also a local minimum)?
- How can we reduce the number of iterations and thus computation time and cost?
- How can we stabilize the above procedure, that it works even with poorly conditioned field data?

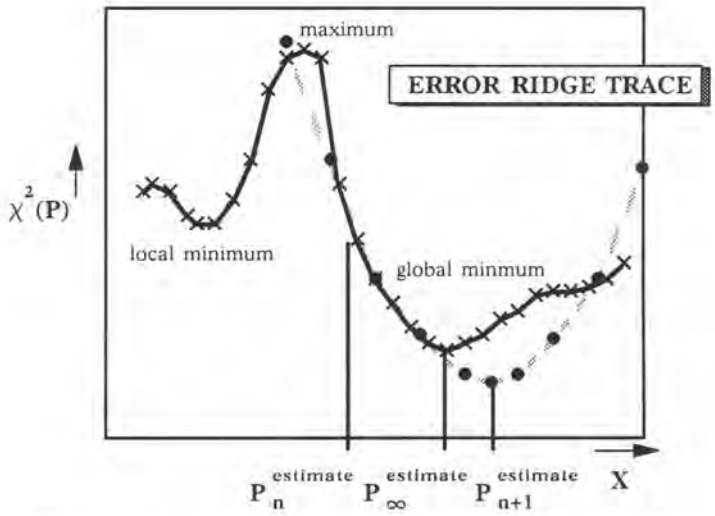

Fig. 4.3: Error ridge trace as function of the estimated model parameters (after Menke, 1984).

The answer to the first question is quite simple: **We don't.** There are two different ways of inverting geophysical data. One way is the mathematically correct way, yielding the best fit model and the other the physically reasonable (which does **not** mean mathematical incorrect!). Since we are, however, dealing with real geology and real noise superimposed on the data, we need to distinguish between mathematically correct and physically reasonable. This is done by using inversion statistics which provides us with error bounds for our results, which can then be used to correlate adjacent stations. As example, if we consider two receiver stations next to each other (500 m apart), both of them have quite noisy signals. One of them yields a conductor at 2 kilometers depth, whereas the other yields a conductor at 4 kilometers depth. Interpretation was done in both ways: The first way – the mathematically correct one – yields a best fit model which is not a consistent model for both stations. The curve fitting error for both stations is below 1%. The other possible solution is a conductor at three kilometers depth at both stations, but the error lies around 10%. The geology, however, tells us that we have a sedimentary basin and the layering is almost horizontal. From this knowledge, a geophysicist would probably justify using the poorer fitting results as the more probable ones. Fortunately, we always have more than just 2 stations and ambiguity is greatly reduced.

The second question can be readily answered with a large variety of techniques. We will in this chapter only consider the *Marquardt–Levenberg method* with the *singular value decomposition*, since most inversion programs use this technique. This leads us directly to the answer of the third question about the inversion stability. In the above mentioned technique a damping factor is introduced to increase the stability of the

inverse. For the following the weighting matrix is dropped which causes no loss of generality.

When the matrix $\mathbf{J}^T\mathbf{J}$ becomes singular ($\det \mathbf{J}^T\mathbf{J} = 0$) we obtain no solution. If $\mathbf{J}^T\mathbf{J}$ is almost singular ($\det \mathbf{J}^T\mathbf{J} << 1$) we obtain oscillations (large parameter variations). These oscillations can be reduced when introducing a damping factor, K, such that equation 4.10 is modified:

$$\Delta \mathbf{p}(\mathbf{J}^T\mathbf{J} + K^2 \mathbf{I}) = \mathbf{J}^T \mathbf{g} \tag{4.12}$$

where I is the identity matrix.

The damping factor can be optimized to achieve very fast convergence, but extreme care should be taken when working with electromagnetic data.

A way of obtaining an evaluation of the parameter resolution is the additional use of the *singular value decomposition* (SVD) or spectral decomposition. The Jacobian is substituted by the product of two orthogonal matrices, **V**, **U**, and one diagonal matrix, **S**, containing the roots or the eigenvalues of **J**, S_i. A detailed description of the SVD can be found in Jackson (1972) and a summary in the appendix.

Let
$$\mathbf{J} = \mathbf{U}\mathbf{S}\mathbf{V}^T \tag{4.13}$$

From equation 4.10 this yields:

$$\Delta \mathbf{p} = (\mathbf{J}^T\mathbf{J})^{-1} \mathbf{J}^T\mathbf{g} = (\mathbf{V}\mathbf{S}\mathbf{U}^T\mathbf{U}\mathbf{S}\mathbf{V}^T)^{-1} \mathbf{V}\mathbf{S}\mathbf{U}^T \mathbf{g} = \mathbf{V}\mathbf{S}^{-1}\mathbf{U}^T\mathbf{g} \tag{4.14}$$

where
$$\mathbf{U}^T\mathbf{U} = \mathbf{V}^T\mathbf{V} = \mathbf{V}\mathbf{V}^T = \mathbf{I}_n \tag{4.15}$$

Equation 4.14 is not defined if one of the singular values equals zero. We therefore introduce the damping factor K for stabilization:

$$\Delta \mathbf{p} = (\mathbf{V}\mathbf{S}^2\mathbf{V}^T + K^2 \mathbf{I}_n)^{-1} \mathbf{V}\mathbf{S}\mathbf{U}^T\mathbf{g} \tag{4.16}$$

or

$$\Delta \mathbf{p} = \mathbf{V} (\mathbf{S}^2 + K^2 \mathbf{I}_n)^{-1} \mathbf{V}^T\mathbf{V}\mathbf{S}\mathbf{U}^T \mathbf{g} \tag{4.17}$$

or

$$\Delta \mathbf{p} = \mathbf{V}\,\mathrm{diag}\left(\frac{S_j}{S_j^2 + K^2} \right) \mathbf{U}^T\mathbf{g} = \mathbf{V}\mathbf{T}\mathbf{S}^*\mathbf{U}^T\mathbf{g} \tag{4.18}$$

where $\mathbf{S}^*$ is defined as

$$S^*_{ii} = \begin{cases} \dfrac{1}{S_{ii}} & \text{for } S_{ii} > 0 \\ 0 & \text{otherwise} \end{cases} \tag{4.19}$$

and $\mathbf{T}^*$ as the damping factors of the transformed parameters

$$T_{ij} = \frac{S_{ij}^2}{S_{ij}^2 + K^2} \tag{4.20}$$

Another advantage of this method is also that the inversion statistics come with the SVD as byproduct.

Resolution Analysis

The **U** and **V** matrices with the orthonormal data space and parameter space eigenvectors can be used to study the resolution of the individual model parameters namely the resistivities and thicknesses. In order to do this the following transformations are used:

$$\mathbf{p} \rightarrow \mathbf{q} = \mathbf{V}^T\mathbf{p} \qquad \text{and} \tag{4.21}$$

$$\mathbf{g} \rightarrow \mathbf{r} = \mathbf{U}^T\mathbf{g} \tag{4.22}$$

Equation (4.21) describes a rotation in the parameter space. The transformed parameters are uncorrelated and the columns of the V matrix describe the linear combinations of the physical parameters for each of the transformed parameters.

The solution of equation (4.12) is obtained by multiplying equation (4.18) with $\mathbf{V}^T$:

$$\Delta\,\mathbf{q} = \mathbf{T}\,\mathbf{S}^*\,\mathbf{r} \tag{4.23}$$

The matrix **T** is important for the progress of the inversion. To demonstrate this, the T_{ii} are normalized by the largest eigenvalue:

with $$\lambda_{ii} = \frac{S_{ii}}{S_{11}} \quad \text{(normalized eigenvalue)} \quad \text{and} \tag{4.24}$$

$$\upsilon = \frac{K}{S_{11}} \quad \text{(normalized damping parameter)} \tag{4.25}$$

we obtain for the T_{ii}:

$$T_{ii} = \frac{\lambda_{ii}^2}{\lambda_i^2 + \upsilon^2} \tag{4.26}$$

The values of T_{ii} control the changes of the transformed parameters. They are dependent on the ratio of normalized eigenvalue and the normalized damping parameter. We thus distinguish between three possible cases:

1. case: $\upsilon \ll \lambda_i$

In this case T_{ii} is about 1 and the respective parameter combination is well resolved.

2. case: $\upsilon >> \lambda_i$

This means T_{ii} becomes small which means that the parameter q_i is changed by only a small fraction. The influence of poorly resolved parameters is strongly damped. Thus the T_{ii} are called *damping factors of the transformed parameters*.

3. case: $\upsilon \approx \lambda_i$

In this case $T_{ii} \approx 0.5$ and the respective parameter is barely damped.

The above considerations show that υ is taking the role of a threshold value for the relative eigenvalues λ_i. Thus υ is commonly set to 0.1 during the initial stage of the inversion. This means that the parameter combinations with eigenvalues less than 10% of the maximum eigenvalues are being damped. The result is that initially only the well resolved parameters are being varied to obtain fast improvement of the fit. Between iterations of an inversion, υ is decreased to consider also the influence of the less resolved parameters. For standard LOTEM inversions we often define 0.01 as lower limit of υ, which means that parameter combinations with less than 1% of the maximum are considered irrelevant.

Jupp and Vozoff (1975) define a class of inversion procedures by setting:

$$T_{ii}^{(N)} = \frac{\lambda_{ii}^{2N}}{\lambda_{ii}^{2N} + \upsilon^{2N}} \tag{4.27}$$

For N = 1 the above described method is obtained. This method is also known as *Marquardt–Levenberg* method. Figure 4.4 shows $T^{(N)}$ as a function of λ for $\upsilon = 1$.

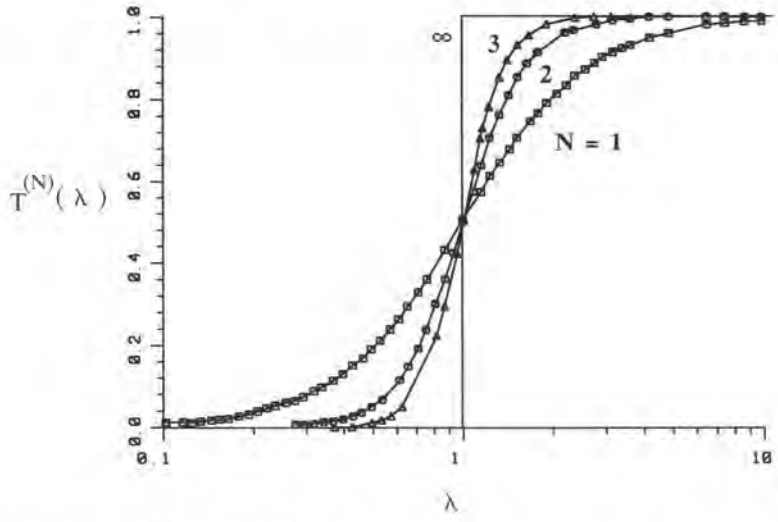

Fig.4.4: The function $T^{(N)}(\lambda) = \frac{\lambda^{(2N)}}{1 + \lambda^{(2N)}}$ for N = 1, 2, 3, ∞ (after Jupp and Vozoff, 1975).

For increasing N higher orders are obtained up to N = ∞ when the influence of parameters with eigenvalues smaller than υ is completely damped.

For LOTEM inversion we use mostly N = 2 which can be termed the *Marquardt–Levenberg method* of second order.

In order to see how well resolved the original parameters are, the damping factors of the transformed parameters are transformed back.

$$\mathbf{T} \rightarrow \mathbf{R} = \mathbf{VT} \tag{4.28}$$

The diagonal elements of **R** are then the *damping factors of the original parameters*. They lie between 0 and 1 and are called *importance* in the inversion statistics. An importance of 1 means that the parameter has strong influence on the fit of the model curve. A small value means that the parameter has little influence on the fit.

Another important quantity for the evaluation of the inversion result is the *number of effective parameters*. It is defined as the sum of the damping factors of the parameters and it is a measure for how many parameters the inversion really resolves.

The solution of the inversion problem depends on the starting model $\mathbf{p}_0$. The reason is that the error function χ^2 can have different minima. This means that quite different earth models satisfy the data equally well. This becomes even more difficult, since there is always noise on the data and the best fit model is not always the one closest to the truth.

Thus, one spends a great deal of time in obtaining as much *a priori* information as possible to eliminate unreasonable solutions. The next step beyond simply comparing the results with well log information is the incorporation of the *a priori* information in the mathematical concept and reduce the bias in the inversion by incorporating other geophysical techniques.

Joint Inversion

In this section the above inversion concepts are extended to inversion of two data sets simultaneously and obtaining only one earth model which satisfies the data set. This type of inversion is called joint inversion. The two data sets may be in principle any type of data which can be interpreted with the same model. For practical purposes we use joint inversion either of two different components of the LOTEM electromagnetic fields or magnetotelluric data and one LOTEM data component.

Using the data sets of two different methods improves in general the results, provided that each data set contains complementary information. Sometimes this means that both data sets must have a large overlapping depth investigation range, sometimes it means that the overlap is small. Since it is possible to obtain different results by the individual interpretation of the components, only careful evaluation can answer the above uncertainty. One always hopes to combine the resolution capabilities of the two methods. Here we have selected the joint inversion of magnetotelluric and LOTEM data because both techniques complement each other well in depth resolution. The

overlap of LOTEM and MT data can readily be compared using the *skin depth* for the MT and the *diffusion depth* for the LOTEM (Spies, 1989).

The mathematical combination of the two methods is obtained by the combination of the matrices but maintaining only one parameter vector (resistivities and thicknesses) such as:

$$\mathbf{y} = \begin{pmatrix} \mathbf{y}_{(\mathrm{LOTEM})} \\ \mathbf{y}_{(\mathrm{MT})} \end{pmatrix} \quad ; \quad \mathbf{J} = \begin{pmatrix} \mathbf{J}_1 \,(\mathrm{LOTEM}) \\ \mathbf{J}_2 \,(\mathrm{MT}) \end{pmatrix} \quad ; \quad \mathbf{f} = \begin{pmatrix} \mathbf{f}_1 \,(\mathrm{LOTEM}) \\ \mathbf{f}_2 \,(\mathrm{MT}) \end{pmatrix} \qquad (4.29)$$

where $\mathbf{y}$ is the data vector containing the field observations, $\mathbf{J}$ is the Jacobian matrix containing the derivatives with respect to the model parameters, and $\mathbf{f}$ is the model function vector containing the forward calculations for a specified model at the same points as the field data.

A problem arises when weighting the data sets: If realistic standard deviations for both data sets exist, none of the data points will be given preference when each data point is weighted with its standard deviation.

With real data, it is often difficult to obtain a realistic error estimate and thus the weights in the weighting matrix are all set equal to 1. Since during the inversion dimensionless parameters are used, both data sets will contribute equally to the solution.

For LOTEM data it is important to include the standard deviation in the inversion because the relative error of the data often deviates by several orders of magnitude. For the joint inversion, if you would like to include the standard deviation for one data set but have no reliable error estimates for the other method, you must normalize the weights. One practical way is to normalize the weights of both data sets by the average of the weights of each data set. This will guarantee an average of the weights which is equal to 1. This means that the data sets are equally weighted against each other but each data set in itself contains its proper weights. For the LOTEM the induction currents at early time are more focused at a certain depth in the subsurface. At later times the induction currents are more spread out and the value at each individual time is more influenced by the values at times before. Thus abrupt weight changes can occur at early times but should not occur at later times.

Next, we will test the joint inversion with synthetic data to demonstrate its usefulness and drawbacks. First both data sets are inverted individually and then jointly. The resolution criteria of the proceeding discussions in this chapter are used. Since below case histories are shown, at this stage synthetic data without noise are used.

The first synthetic data were calculated for a K-type model (low - high - low resistivity, $\rho_1 \leq \rho_2 \geq \rho_3$):

$\rho_1 = 10\ \Omega\ \mathrm{m}$ $\quad$ $h_1 = 2000\ \mathrm{m}$
$\rho_2 = 500\ \Omega\ \mathrm{m}$ $\quad$ $h_2 = 500\ \mathrm{m}$
$\rho_3 = 10\ \Omega\ \mathrm{m}$

In this model, a more resistive layer is embedded between two conductors. Since the magnetic field component of LOTEM has little sensitivity to resistive layers we use the electric field component. We hope for an increased resolution for this type of model with joint inversion, since the MT data will resolve the lower conductor better than the LOTEM data, but MT has little information on the resistive layer which the LOTEM has.

Figure 4.5 shows the synthetic data for the LOTEM (top left) and MT (bottom left). For LOTEM the response of the electric component (in x-direction) was calculated for an offset of 7000 m with the receiver being located on the dipole equator. It shows little structure due to the embedded resistor. The MT apparent resistivity and phase curves show even less structure than the LOTEM curve. The solid line through the data curves shows the result of the joint inversion. The starting model for the individual inversions and the joint inversion was:

$\rho_1 = 50\ \Omega$ m $h_1 = 1800$ m
$\rho_2 = 50\ \Omega$ m $h_2 = 1000$ m
$\rho_3 = 50\ \Omega$ m

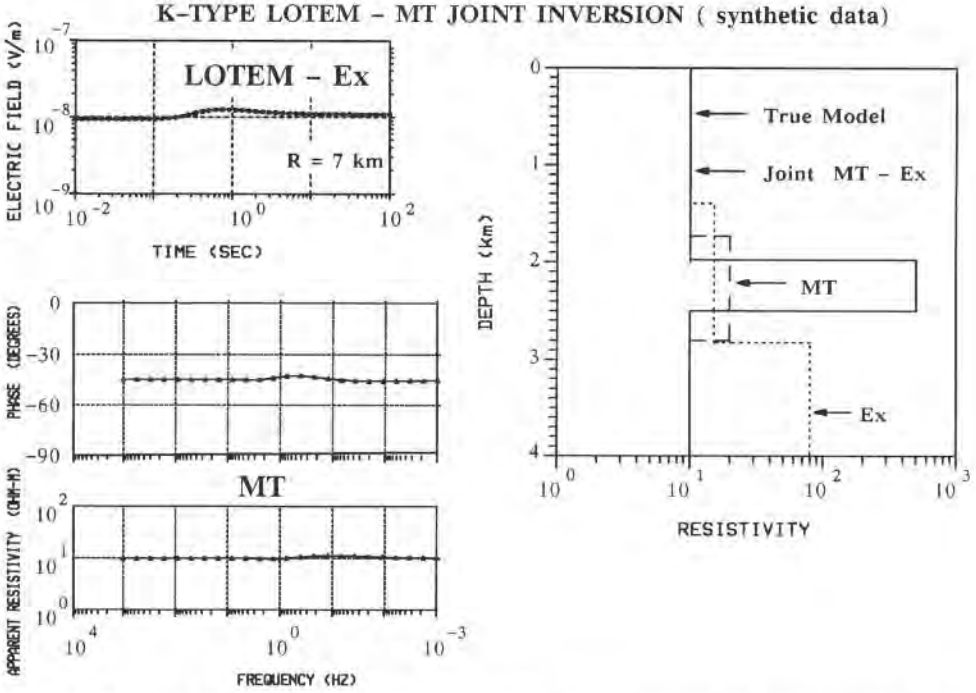

Fig. 4.5: Synthetic data example for LOTEM and MT joint inversion for a K-type model (left) and inversion results on the right. The joint inversion result here is the same as the true model (after Hördt, 1989).

The comparison of the results is shown in Figure 4.6. The MT data sees a thick slightly resistive layer whereas the LOTEM electric field is sensitive to an increase in resistivity. The LOTEM reaches higher resistivities than the MT, but never penetrates through the resistor. Only the joint inversion resolves the resistor. A difference between the original model and the inversion result is not visible. The fit for all three inversions is better than 1 %. If the interpreter had only one of the techniques available to him he would have difficulties finding the true model without the joint inversion. The higher quality of the joint inversion result can be shown using the V matrix (which relates the physical and the transformed parameters) as displayed in figure 4.6.

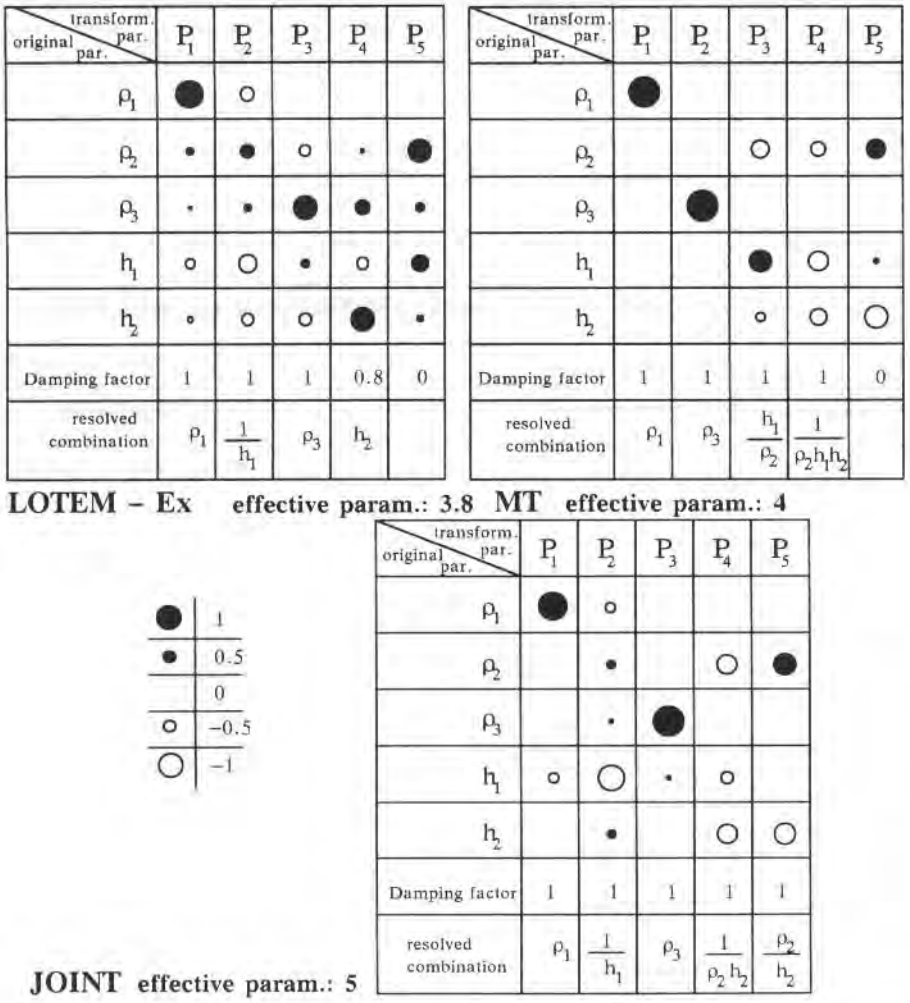

Fig. 4.6: V matrices for the individual and joint inversion of LOTEM and MT data using K-type synthetic data (after Hördt, 1989).

The relation between the transformed parameters P and the original parameters of the model is obtained by adding the logarithms of the original parameters multiplied by the coefficient. In figure 4.6 for the LOTEM electric field and the first transformed parameter P_1 we obtain:

$$P_1 = 0.88 \log(\rho_1) + 0.25 \log(\rho_2) + 0.11 \log(\rho_1) - 0.33 \log(h_1) - 0.19 \log(h_2) \qquad (4.30)$$

This means that the parameter combination $\dfrac{\rho_1^{0.88}\rho_2^{0.25}\rho_3^{0.11}}{h_1^{0.33}h_2^{0.19}}$ is resolved.

The circles in figure 4.6 represent the coefficients of the transformed parameters. The circle diameter is proportional to the coefficient which is between 0 and 1. Open circles mean negative coefficient. The dominating parameter is the resistivity of the first layer. From the matrix of the electric field it can also be seen that the electric field sees the increasing resistivity but not the structure. This effect is independent of the starting model and even when the starting model is close to the true model the resistive layer will not be resolved. The joint inversion combines the resolution of both individual inversions and more parameters are resolved as can be seen at the bottom of the figure.

The second case considers an A-type (increasing resistivity with depth, $\rho_1 \leq \rho_2 \leq \rho_3$) model and the combinations of LOTEM magnetic field data with MT. This is a less favourable condition as the last one because neither the MT nor LOTEM magnetic field have full capabilities to resolve resistors. However, the combination should bridge the typical gap in the MT signal around 1 Hz. Both data sets the MT data and the LOTEM magnetic component have similar sensitivities to the subsurface resistivity. The model consists of three layers:

$\rho_1 = 10\ \Omega$ m $h_1 = 800$ m
$\rho_2 = 100\ \Omega$ m $h_2 = 2000$ m
$\rho_3 = 1000\ \Omega$ m

The model type is very typical because the resistivity often increases with increasing depth for a depth range between 1 and 20 km. Figure 4.7 shows the synthetic data for LOTEM magnetic field (top left) and the MT measurements (bottom left). For the MT, the data around 1 Hz (0.25 Hz to 8 Hz) has been eliminated, because in this frequency range the natural source signal is generally very weak.

The inversion results are presented on the right of figure 4.7. The MT inversion did not change the parameters of the second layer which is caused by the gap in the data. The LOTEM magnetic field and the joint inversion give approximately the same results. In order to better evaluate this, one can consider the damping factors of the original parameters – also called importances – as shown on the bottom right of figure 4.7. The joint inversion resolves more layer parameters. Contrary to the previous example, this result depends upon the starting model, in particular the values of the

importance of the second layer. In this case this dependence can be explained by the non-linearity in the solution and the instability of linearized inversion.

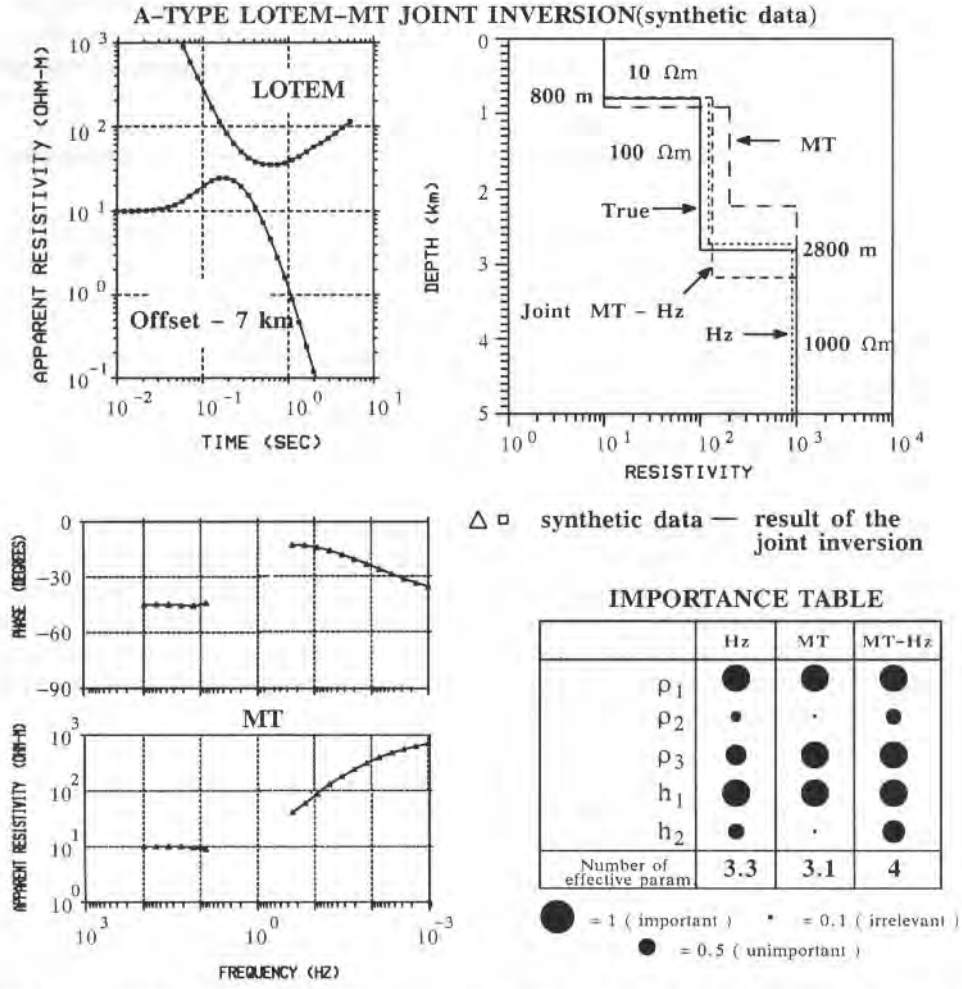

Fig. 4.7: LOTEM (top left) and MT (bottom left) synthetic data for an A-type model. On the right inversion result are shown with the parameter importances below (after Hördt, 1989).

Apart from the above shown examples, further tests were done for Q-type (decreasing resistivity, $\rho_1 \geq \rho_2 \geq \rho_3$) and H-type (imbedded conductor, $\rho_1 \geq \rho_2 \leq \rho_3$) models. In both cases the joint inversion did not improve the result. On the other hand, it was also not worse than the individual interpretation.

Following, one brief case history of jointly interpreting MT and LOTEM data is shown. Both data sets were measured in the area around the Münsterland borehole in

North–Western Germany (Hördt, 1989). A more detailed interpretation case history is shown later on. Here, only methodological aspects are considered. Figure 4.8 shows the real field data for the LOTEM magnetic field measurements. The MT consists of a combination of controlled source audio magnetotelluric (CSAMT) and MT data. The solid lines through the data represent the results of the joint inversion. In both cases – the MT and LOTEM – a better fit could be obtained with the individual inversions. However, it is not certain that the resulting model would be more realistic.

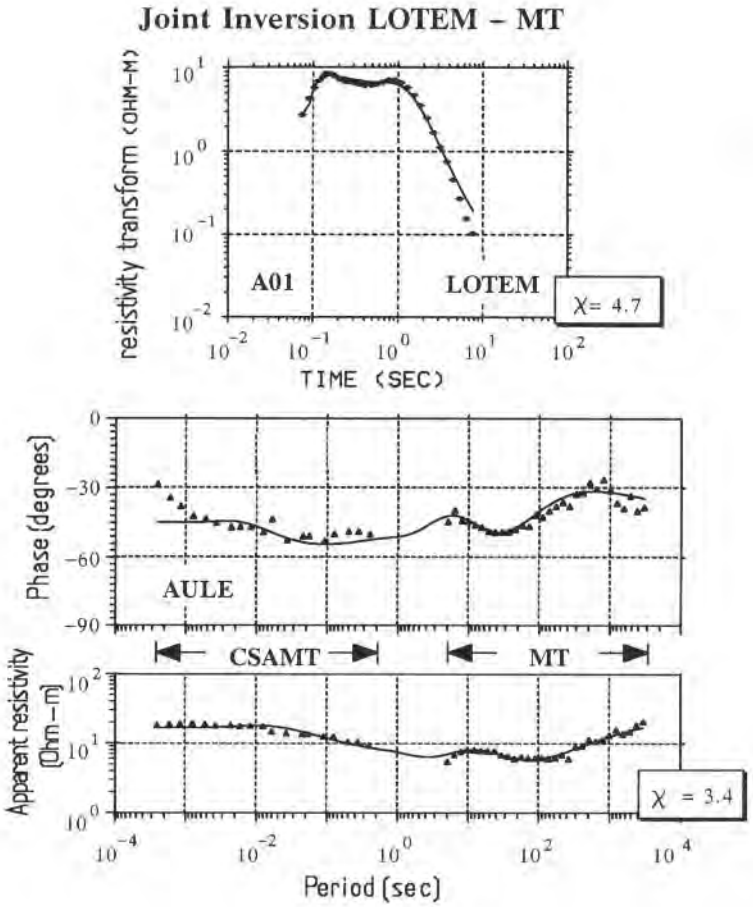

Fig. 4.8: Field data for LOTEM (top) and MT (bottom) measured at the same site in North–Western Germany with the synthetic curves for the joint inversion result (after Hördt, 1989).

Figure 4.9 compares the individual inversion and the joint inversion results with the well log. The joint inversion result fits the well log best and MT and LOTEM complement each other in depth investigation range. Still, there is some deviation from the well log which can be explained with three–dimensional structures. They lie

mainly in the gradual resistivity increase (see well log), where the layered earth model is inappropriate and will be discussed in more detail later on.

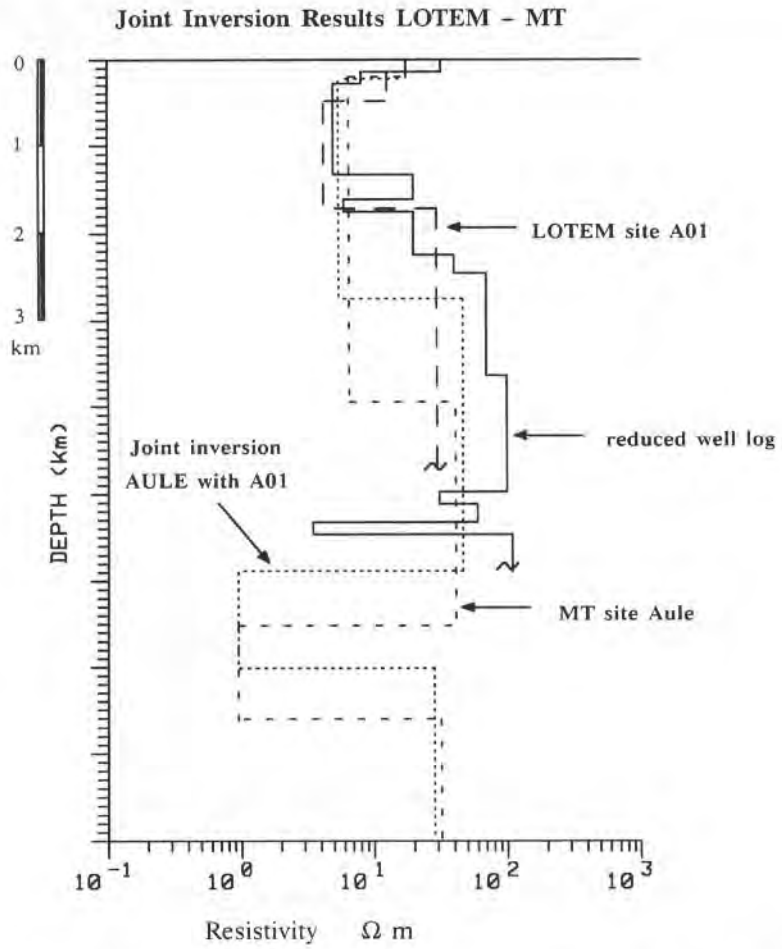

Fig. 4.9: Comparison of the individual inversions and the joint inversion with the well log (after Hördt, 1989). The reduced well log was derived from blocking of the original laterolog (Büchter, 1983).

Profile Inversion

When interpreting several soundings along a profile, the interpreter is comparing the individual inversion results with the results of the adjacent soundings. In a sedimentary environment, one mostly interprets the data in terms of layered earth models and is searching for deviations from the layering. If the inversion result of one station varies only slightly from the adjacent ones, the interpreter moves onto the next sounding. If the inversion result at one station varies significantly from the available adjacent stations, there is either a problem with the data (such as processing, scaling or noise) or the geology (e.g. 3–D structure, fault). These soundings take up most of the interpretation time since one has to make sure the problem with this particular data is analyzed and all possible inversion models have been tried. This is a very slow process requiring significant user interaction. Automatically, one requests a technique to carry out the inversion along a profile on the computer and thus reduce the user interaction to the data set where the standard inversion is not successful. We call such a procedure *profile inversion*.

The goal for such kind of procedure is to derive a more objective criterion to aid the interpreter. To achieve this, two tasks can be defined:

- One must find a reliable model for a profile.
- The results from one station must be objectively transferred to the next station.

The derivation of a reliable model for a station can be done in many different ways. The best way is the use of a good complete well log and an exemplary cross check with one station. If no additional information is available the interpreter is left to his own judgement and needs to find the reliable model on a trial and error basis. Once the model has been defined the *profile inversion* can be used.

The transfer of information from one station to the next in the inversion process can be done in many different ways. The simplest way is to use the last inversion result as input for the next station. The checks can be done with simple parameter comparison. This procedure will, however, only be successful in areas with very simple geology and not save much interpretation time. Here, we also consider two approaches to integrate the results from one station for the next station more thoroughly. The first approach is called *inversion with soft bounds* and the second *inversion with hard bounds*. The latter will mainly be considered theoretically, since not enough experience exists in applying the hard bounds inversion to field data. The derivation is following closely Petry (1987) with a more mathematical description given by Lawson and Hanson (1974).

In the derivation we start with a simplification of equation (4.10)

$$\mathbf{W}\,\mathbf{J}\,\Delta\mathbf{p} = \mathbf{W}\,\mathbf{g} \tag{4.31}$$

If we define a weighted Jacobian such as $\mathbf{W}\,\mathbf{J} := \mathbf{J}_W$ we obtain

$$\mathbf{J}_W \, \Delta \mathbf{p} = \mathbf{W}\,\mathbf{g} \tag{4.31}$$

where $\mathbf{J}_W$ is an n x m matrix and Δ the parameter difference vector containing m values for the parameters. We now append to the Jacobian an n x n diagonal matrix, **D**, which contains the parameter weights on the main diagonal normalized by m/n. To the discrepancy vector a Nullvector, **0** of length n, is appended. Equation (4.31) converts then to:

$$\begin{pmatrix} \mathbf{J}_W \\ \mathbf{D} \end{pmatrix} \Delta \mathbf{p} = \begin{pmatrix} \mathbf{W}\,\mathbf{g} \\ \mathbf{O} \end{pmatrix} \tag{4.32}$$

where

$$\mathbf{D} = \text{diag}\left(\frac{m}{n}\, u_i\right) \qquad i = 1, \ldots, m \tag{4.33}$$

contains the non-negative weights of the i-th parameter u_i. The boundary condition – meaning that the parameter changes between stations are small – is described by:

$$\mathbf{D}\,\Delta\mathbf{p} = \mathbf{O} \tag{4.34}$$

This is exactly what we wanted: parameters with large weights are changed little and parameters with small weights can be modified more during inversion.

For hard bounds one would like to constrain the parameters explicitly within a given range. This range can be derived from well logs or other information. For a start parameter $\mathbf{P}_0$, an upper and lower bound is defined such as upper bounds: $\mathbf{P}_0 + \mathbf{P}^u$ lower bounds: $\mathbf{P}_0 + \mathbf{P}^L$ (Weidelt, pers. comm.).

The i-th component of the parameter vector **P** is then calculated in the k-th iteration by

$$P_{K,i} = P_{0,i} + \frac{P_i^u - P_i^L}{2} + \frac{P_i^u + P_i^L}{\pi} \arctan\left(a\, x_{K-1,i}\right) \tag{4.35}$$

where x_k is the sum of the undamped parameter variations during the k iterations. Instead of inverting for the parameter change during one iteration, $\Delta\mathbf{p}$, the inversion is now done with the total parameter change of x_k. Including the arcus-tangent function in this way guarantees that P does not penetrate the bounds. The new Jacobian consists then of:

$$\frac{\delta f_j(\mathbf{P})}{\delta x_i} = \frac{P_i^u + P_i^L}{\pi} \frac{a}{1 + a^2 x_i^2} \frac{\delta f_j(\mathbf{P})}{\delta p_i} \tag{4.36}$$

The factor, a, directs the convergence. A large factor causes fast move away from the starting value but a slow convergence when the result is close to the final solution.

The first *profile inversion* case history uses data from a sedimentary basin in Europe. The basin is known to be approximately horizontally layered. Figure 4.10 shows three different inversion results for the same survey line. The field data was of average quality and a representative for the area. For the top of figure 4.10 the same starting model was used for the inversion of all soundings. This model was:

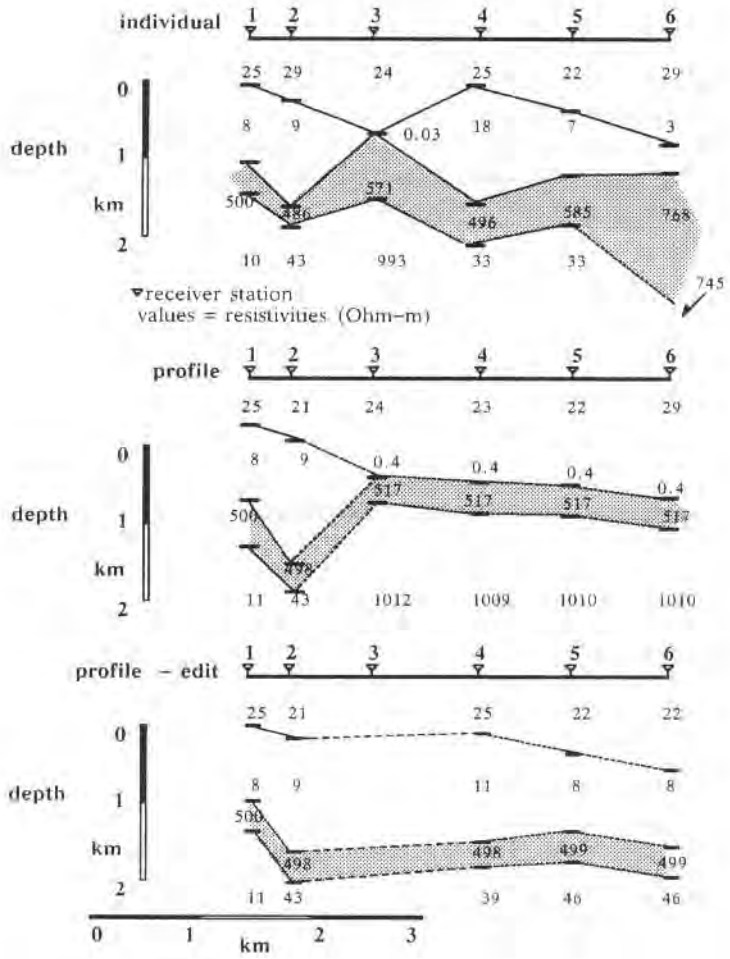

Fig.4.10: Inversion results for the same survey line. The top shows the results of the individual inversions using the same starting model for all data. The middle is the same line when the inversion result of the previous station was used as starting model for the next station. The bottom frame shows the results of the same procedure after eliminating station 3 (after Petry, 1987).

ρ_1 = 20 Ωm h_1 = 800 m
ρ_2 = 10 Ωm h_2 = 1100 m
ρ_3 = 500 Ωm h_3 = 400 m
ρ_4 = 30 Ωm

Notably, the structure from the inversion models is erratic when using the shaded area as tracing layer. In particular, the result from station 3 is different from the expectations (known from well logs). The conductive second layer has been reduced to a very thin very conductive layer. The middle of figure 4.10 shows the results after applying a simple version of the *profile inversion* where the final model (inversion result) of the previous station is used as starting model for the next station. The structure becomes smoother, but the values of station 3 are still quite different from the expectations. After eliminating station 3, the section displayed at the bottom of figure 4.10 resulted. The elimination of station 3 was justified by the noise level in the data. The structure is significantly smoother.

Figure 4.11 shows the result using soft and hard bounds. The soft bounds (top) were applied using the following weights for the layer parameters:

ρ_1 : 1. – fixed h_1 : 1. – fixed
ρ_2 : 1. – fixed h_2 : 0.5 – constrained
ρ_3 : 0.05 – free h_3 : 0.1 – free
ρ_4 : 0.1 – free

These weights were chosen, because the magnetic field measurement does not well resolve the resistive layer. The weight for the thickness of the second layer was derived after seeing in the previous inversions that the result is strongly biased towards the well resolved conductor. The second layer thickness was reasonably well known from well log data.

The resulting model is very smooth. The top of the figure shows the results after applying the hard bounds algorithm. For the hard bounds the following tolerances were used for the model parameters:

ρ_1 : ± 50% h_1 : ± 25%
ρ_2 : ± 25% h_2 : ± 50%
ρ_3 : ± 60% h_3 : ± 90%
ρ_4 : ± 90%

The result is smooth, however, it shows a slope towards station 6 which could be systematic or is required by the data.

These values were derived from the knowledge of the results in figure 4.10 and the true resistivities of the subsurface measured in a borehole. For both cases, the structure is now very smooth and represents closely the true resistivity distribution, but deviates in the thicknesses. The hard bounds force the data to a higher degree to match the preconceptions of the interpreter.

The sections using the hard and soft bounds are more realistic compared with the results in figure 4.10. They were also automatically calculated without user interaction. However, the data fit in both sections is worse than for the section in figure 4.10. Thus extreme care should be taken when applying this procedure and it should only be used when good structural constrains (i.e. well logs) exists.

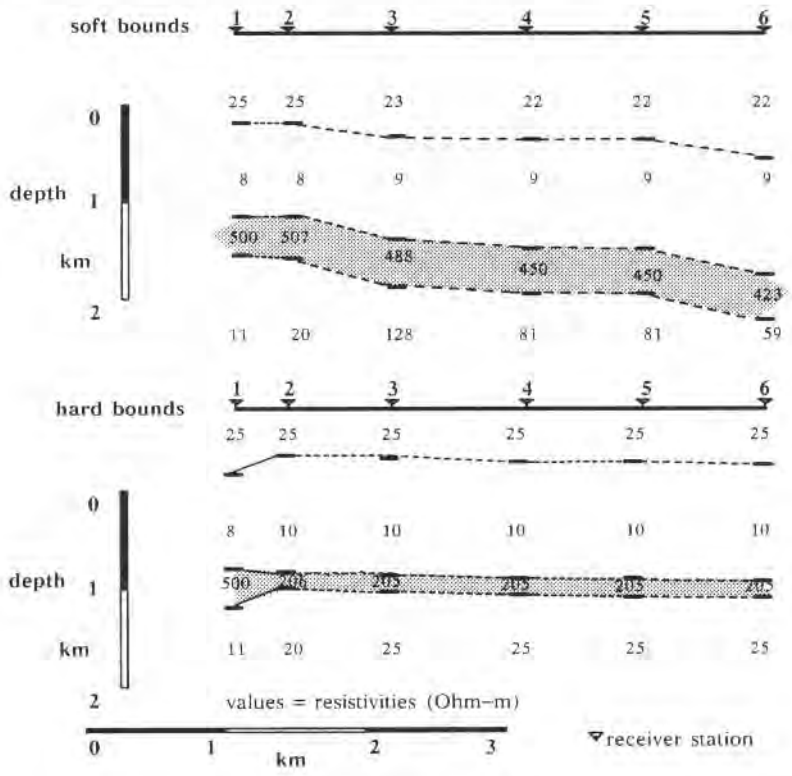

Fig.4.11: Inversion results for the same data as in figure 4.10 using soft bounds (bottom) and hard bounds (top) *profile inversion* (after Petry, 1987).

The next case history is for a data set from North-Western Germany. The data was interpreted using the above inversion procedures. Figure 4.12 shows the interpreted resistivity section from the one-dimensional inversions without consideration of the adjacent stations. For all stations the following starting model was used:

ρ_1 = 13 Ωm h_1 = 300 Ωm
ρ_2 = 5 Ωm h_2 = 1000 Ωm
ρ_3 = 15 Ωm

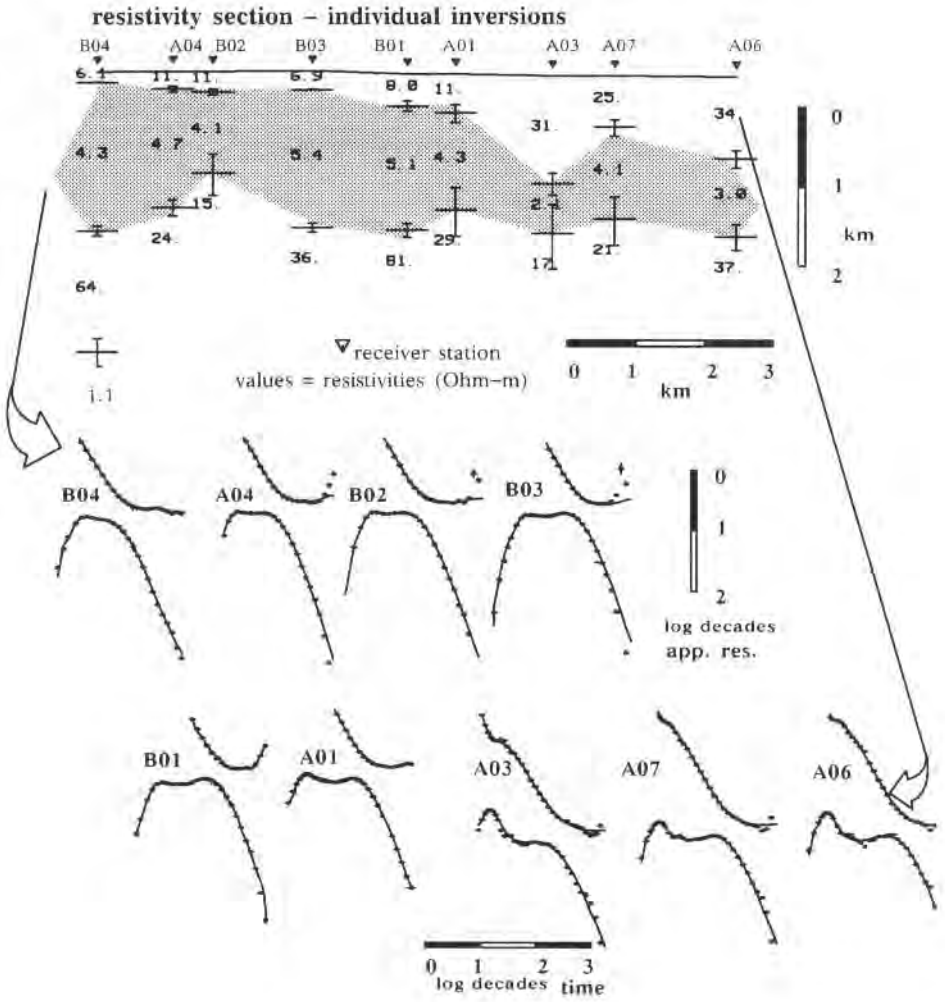

Fig. 4.12: Interpreted resistivity section using the individual inversion results (top). At the bottom of the figure the data (squares) and synthetic curves are shown sequentially starting from the left side of the profile.

This model was derived from well log reduction of a 6 km deep borehole and subsequent forward modeling to obtain the minimum number of resolvable layers. The six stations on the left of the figure give reasonably consistent results whereas the resistivity section is jagged on the right side of the figure (inconsistency of the model). Below the section, the data (squares) is displayed with the solid lines representing the synthetic curves for the corresponding earth model. The three stations at the right side of the profile, A03, A07 and A06 are influenced by distortion in the field data which

can be seen in the high bend at early times. Most likely this distortion is caused by a three-dimensional effect. The data are, however, well fit by a one-dimensional model.

Figure 4.13 shows the results of the simple *profile inversion* when the final model of the previous station was used as starting model for the next station. The structure in

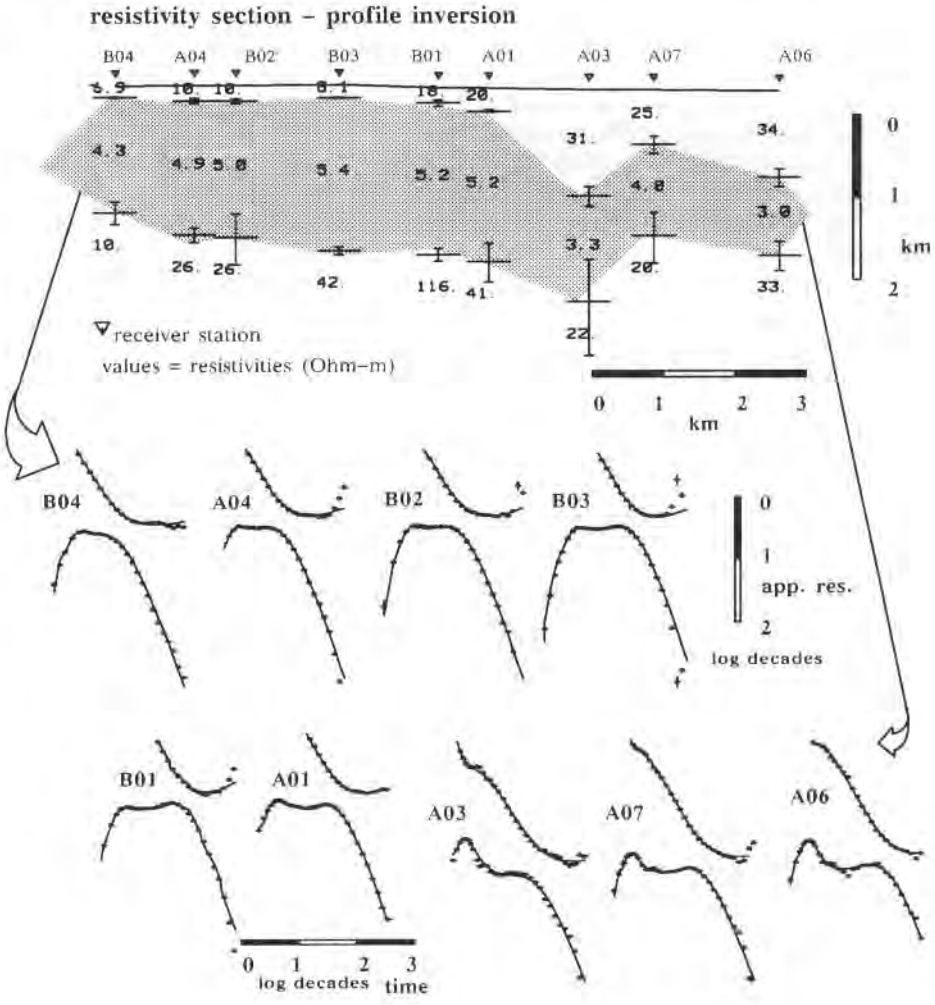

Fig.4.13: Interpreted resistivity section for the *profile inversion* without parameter bounds. At the bottom of the figure the data (squares) and synthetic curves are shown sequentially starting from the left side of the profile.

the resistivity section becomes already smoother including the right part of the profile. The data at the bottom of the figure shows only slightly worse data fits at later times.

The error bars for the layer thicknesses have essentially stayed the same except for station A03.

Figure 4.14 shows the resistivity section for the *profile inversion* when soft bounds were used. Since the resistivity of the second layer is well known, this layer has the highest weights. The detailed weights for the model parameters are:

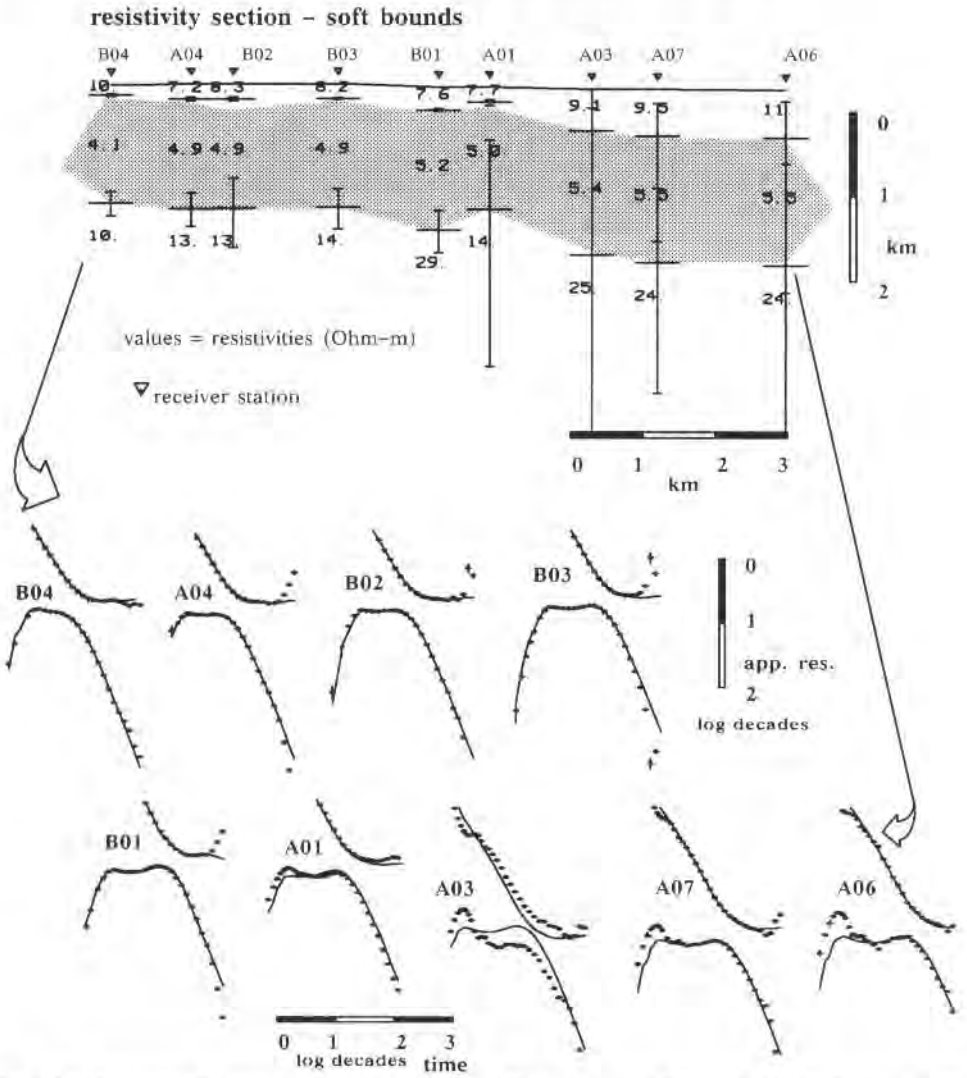

Fig.4.14: Interpreted resistivity section using the profile inversion with bounds. At the bottom of the figure the data (squares) and synthetic curves are shown sequentially as indicated by the arrows.

ρ_1 : 0.5 h_1 : 0.5
ρ_2 : 2. h_2 : 1.
ρ_3 : 0.5

The starting model was consistent with the borehole measurements. The result is even smoother than the section shown in figure 4.13. However, the data fit is not as good. In many instances the inversion terminated at the maximum number of iterations and not upon convergence. This is also expressed in the larger error bars for almost all curves.

In general the weighted *profile inversion* fits the geology better than the individual inversions. However, one cannot neglect that this fit is somehow forced and extreme care should be taken. In particular, a detailed analysis of the inversion statistics and the noise characteristics of the data becomes essential. When three-dimensional geology exists the *profile inversion* may serve to continue the underlying 1-D geology over the local 3-D anomaly. This procedure must be backed by 3-D modeling.

Occam Inversion

In the above chapter we have seen that we can interpret the field measurements along a profile and thus give the interpreter another tool to derive his/her more objective judgement. However, one needs a tool which shows which kind of information is actually in the data, and which is a result of the interpreters influence. Thus we are still looking for an even more objective tool to interpret the data. While searching for this, we must also consider the problems in our assumption. When inverting data to a minimum error, we are assuming that a specific number of layers will fit the data. However, the geology consists – if at all layered – of many layers and in most instances the resistivity changes between the layers are discontinuous on the scale of centimeters, but when the layers are lumped together in tens or hundred of meters they are, in sedimentary areas, mostly continuous. This assumption is no longer valid when a strong contrast of thick units exists (e.g. salt-sediment boundary; sediments above basement; crystalline units). For a smooth resistivity model we consider the concept of *Occam Inversion* which was first reported by Constable et al (1987). We will follow their concept closely and demonstrate the usefulness of *Occam inversion* with some case histories.

The *Occam Inversion* is based on the assumption that the resistivity – depth structure should be as smooth as possible. This means one is trying to avoid the jagged structures and is simply trying to fit the data with a smooth model. Even before looking at the mathematics it becomes evident that this will significantly increase the computation time. The assumption of a minimum model will, however, reduce the possibility of overinterpretation.

When inverting data we are generally speaking of a least squares process under boundary conditions. This means the functional to be minimized, F, consists of a

quantity to be minimized, Q, and an expression, P, describing the boundary conditions.

$$F = Q + P \tag{4.37}$$

The boundary condition term is multiplied with the Lagrange multiplier. The choice of the boundary condition determines the method used. For the Marquardt inversion, Q is the weighted least squares error, and P restricts the parameter change during the iterations. For the *Occam inversion* one requires smoothness of the resistivity – depth function in terms of roughness. The roughness is the integrated square of the first or second derivative with respect to depth (Constable et al, 1987).

$$Q = \chi^2$$

$$P = R_1 = \int \left(\frac{dm}{dz} \right)^2 dz \tag{4.38}$$

or

$$P = R_2 = \int \left(\frac{d^2m}{dz^2} \right)^2 dz \tag{4.39}$$

where R_1 and R_2 are the respective roughness of first or second order; m(z) is here the resistivity versus depth function. The roughness should be as small as possible during inversion. As in the above chapters, one must minimize the χ^2. However, since perfect fits are almost never achievable with real data the iterative process continues until the χ^2 value falls below a predefined threshold value. As one approaches small values of χ^2, a substantial increase in roughness is required for little improvements (Parker, 1984). For further detailed derivation of the mathematics the reader is referred to Constable et al (1987).

The first case history is from a basalt covered area in Western Europe. Very little is known about the geology below the basalt, except that there are some sediments below. Without borehole information, the interpretation of LOTEM data becomes difficult, since one does not know how many layers one needs for the interpretation. Figure 4.15 shows a comparison of the *Occam inversion* with a three or four–layer model. The *Occam inversion* shows a smooth curve exhibiting a conductor. The center of the conductor is several hundred meters deeper than the center of the two–layer earth models. This indicates that either the assumption of layering in the Marquardt solution is insufficient or there are systematic problems in the data. Another possibility could be that the change from the top layer (basalt) to the strata below (interpreted as sediments) is abrupt. From this figure no judgement as to which one is correct can be made. Since the Occam model is unique, this example illustrates how the *Occam inversion* can be used to correlate the layered earth models and select the most likely result. In this case one should not trust any layered earth model without additional geological confirmation.

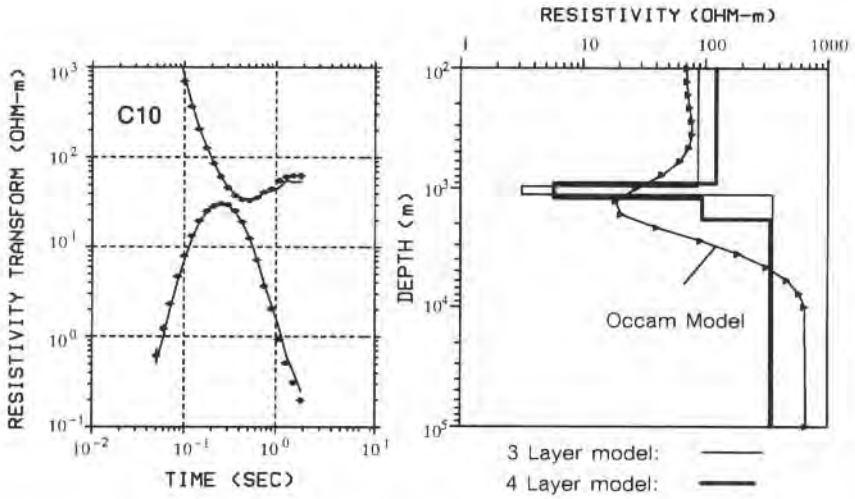

Fig.4.15: Comparison of *Occam inversion* with layered earth inversion. The left frame shows the field data (squares) with the theoretical curves for the inversion results on the right (smooth curve) (after Schruth, 1990).

Figure 4.16 shows an additional example of an *Occam inversion* for data from North-Western Germany. Since the display of a smooth earth model leaves the question open where to anchor the layer value on the graph, the Occam model is now

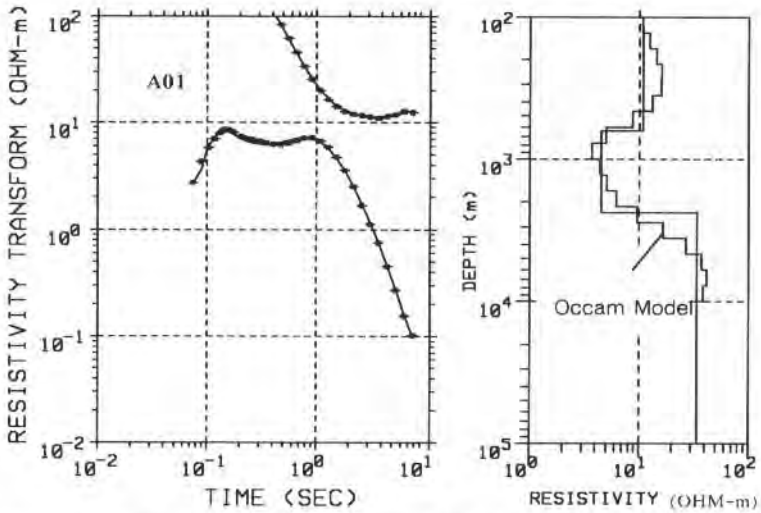

Fig.4.16: Example of an *Occam inversion* compared with the layered earth inversion result.

plotted as multi-layer model which is also the way it is calculated in the inversion program. Here, the Occam result nicely confirms the layered earth interpretation. Thus for this type of data, layered interpretation is sufficient, whereas for the previous example both inversions were needed to verify the existence of the conductive layer.

Figure A.7.1 (appendix 7) shows the result of applying the *Occam inversion* along an entire profile. The resulting model at each station is colour contoured. The top of the figure shows the resistivity depth section of the inversion results as output and displayed as colour section. Notably one can already recognize a detailed structure and consistency between the stations. However, some inconsistencies in particular at later times (greater depth) when the signal-to-noise ratio becomes worse is visible. Thus a lowpass filter is applied to the data horizontally. The filter width is half of the depth. The section in the middle of figure A.7.1 is smoother than the top. The overall structure (overthrusting) is more visible than in the top display of the figure.

The above examples have shown the usefulness of the *Occam inversion*. It can be applied to find problems in the interpretation or to verify the interpretation. Along a profile it can be used to obtain an interpretation which honors the data more than a layered earth interpretation. However, since many layers are used in the forward algorithm and the inversion goes through many iterations, the *Occam inversion* is very computation time intensive and cannot be used as a routine tool (figure 4.17 took about 50 hours CPU time on a MicroVax II; 12 hours with array processor).

INTERPRETATION OF DISTORTED TRANSIENTS (REVERSALS)

When carrying out field measurements sometimes signals are being recorded which do not conform with the type of signal expected from theory. These signals are called distorted signals. A common form of a distorted signal is a transient which changes polarity during the transient duration. This means that the signal crosses its DC level which is used as reference zero level. These transients are called *reversals*. Reversals are theoretically not possible for layered earth structures. They are indicative of three-dimensional structures or strong cultural noise sources (i.e. pipelines, railroad tracks, etc.). In this section the present understanding of reversals is addressed yielding the following questions:

- What is a reversal?
- How do we deal with data with reversals?
- How do we simulate reversals?

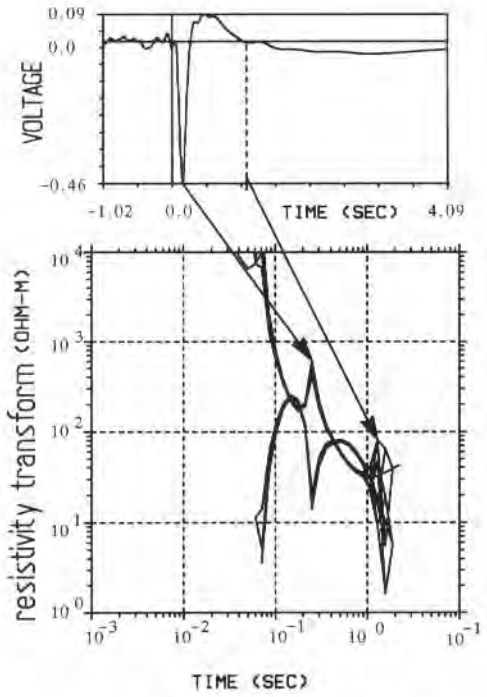

Fig.4.17: Display of observed field data showing a reversal. The top is the linear display of the stacked transients and the bottom a logarithmic display after apparent resistivity conversion. The crosshatching represents the 95% confidence interval.

So far, as field data interpretation is concerned, reversals have only been qualitatively interpreted. Two examples of interpreting reversals taken from Stoyer and Damron (1986) and Stephan (1989) are given.

A distorted transient is a transient which behaves differently from the expected exponential decay over a layered earth. Sometimes when it crosses the reference level it is difficult to decide which part of the transient is the reverse part and which part is the non-reverse part. Figure 4.17 shows an example for a transient which has a sign reversal. The top of the figure shows the linear voltage versus time display of the stacked transient as recorded and observed in the field, the bottom figure displays the data after further poststack processing and conversion to early and late time apparent resistivity transforms. This reversal is a strong onset-reversal which means the reversal starts directly after the onset. Sometimes a reversal consists of a small onset reversal which is significantly smaller than the transient. In figure 4.17 the second reversal at later times could be either caused by incorrect reference level determination or additional three-dimensional effects. The insufficient reference level determination is sometimes the result of strong cultural noise and a reversed onset which can make an

objective judgement of the DC-level for the interpreter almost impossible. Reversals are easily recognized in the field, but not so easily classified.

Stoyer and Damron (1986) interpreted field data from a LOTEM survey in the Milford Valley, Utah. They classified their field data distortions into early time reversals, mid-time depressions, mid-time reversals and late time reversals. Late time reversals are sign changes occurring in that part of the apparent resistivity transform which should decay with $t^{-5/2}$. Early and mid-time reversals occur before the roll over time. Example data for the different classifications is shown in figure 4.18.

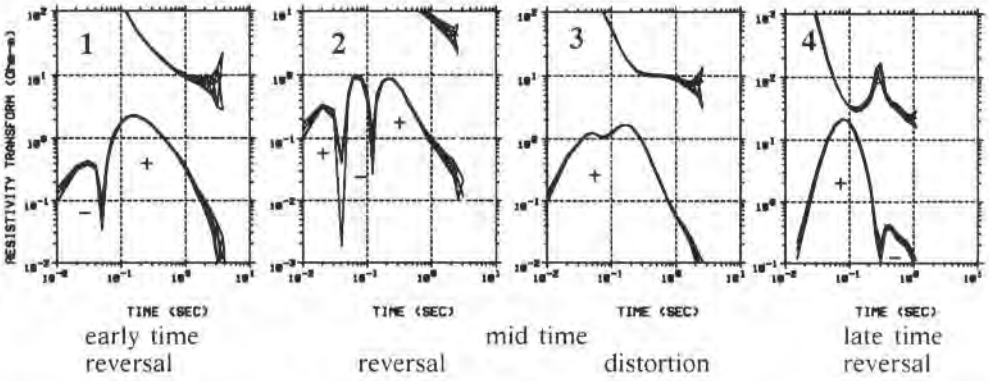

Fig.4.18: Classification of the field data distortions of a LOTEM survey in Utah. The left curve shows a reversed voltage at early times (1) and the right curve at late times (4). The two middle curves show mid-time distortions with a reversed voltage on the left (2) and a strong depression on the right (3) (modified after Stoyer and Damron, 1986).

The classifications are based on the time range when voltage reversals occur. In addition to the reversals there are also strong depressions in the signal which cannot be explained with layered earth interpretation. Stoyer and Damron (1986) used two different approaches to interpret their data. For late time reversals the geology could be explained using an axial conductor in a numerical modeling program (Tsubota, 1979). Figure 4.19 shows the results of Tsubota's calculations inferred for the field data. The axial conductor is buried in a homogeneous half-space. One curve shows the homogeneous earth response (upper curve) and below is the response of the axial conductor. The total field curve is a combination of both. The difference between the total field in figure 4.19 and the late time reversal in figure 4.18 is caused by the system response which has not been removed in figure 4.18 for the resistivity transforms. In figure 4.19 the synthetic data do not consider any system response. Furthermore, the synthetic data were obtained for a half-space host whereas the field data represents a layered host with three-dimensional structure. Considering this, the real field data of figure 4.18 (the late time reversal curve (4)) matches the synthetic results of figure 4.19 well.

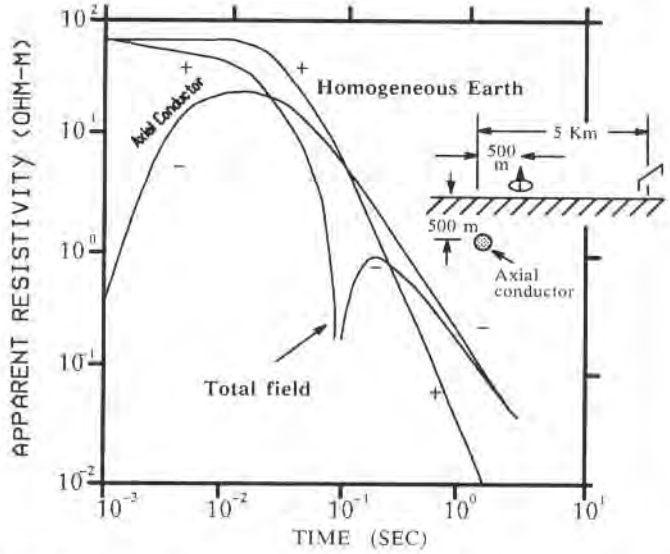

Fig.4.19: Synthetic distorted curve inferred for the Milford data (after Tsubota, 1979; Stoyer and Damron, 1986). The response of the conductor is negative for all times and responsible for the late time reversal. The conductor response is superimposed on the half-space response which is positive for all times.

Using the data classification in figure 4.18 and the synthetic data of Tsubota (1979) in figure 4.19 the soundings at the sites shown in figure 4.20 could be interpreted. A conductor was placed where shown in the figure (right side). The calculated homogeneous earth response, the response of the conductor and the total response are drawn. The total response shows a sign reversal at times when the negative response of the conductor becomes stronger than the homogeneous earth response. This axial conductor is very close to the Negro Mag Fault which is known to contain saline fluids from the geothermal field in the area. Due to the presence of these fluids a conductive anomaly can be expected. Numerical modeling results for this data set is shown below.

Other parts of the field data could not be interpreted in the same manner, because the geologic situation was different. To interpret these data, Damron (1986) built an analog scale model. For normalization and data comparison purposes he used a scaled transmitter – receiver array in a varying offset mode. This means the transmitter is kept fixed while the receiver is moved. The array was moved over a fault simulated by a soldering joint between two metal plates. The soldering joint simulates a more resistive fault zone. Figure 4.21 summarizes Damron's results. The early time curves are asymmetric with respect to the solder joint. When approaching the fault (curves 2 and 3 in figure 4.11) first a depression is seen growing to a mid-time reversal. As the receiver crosses and passes beyond the solder joint, the disturbances change character

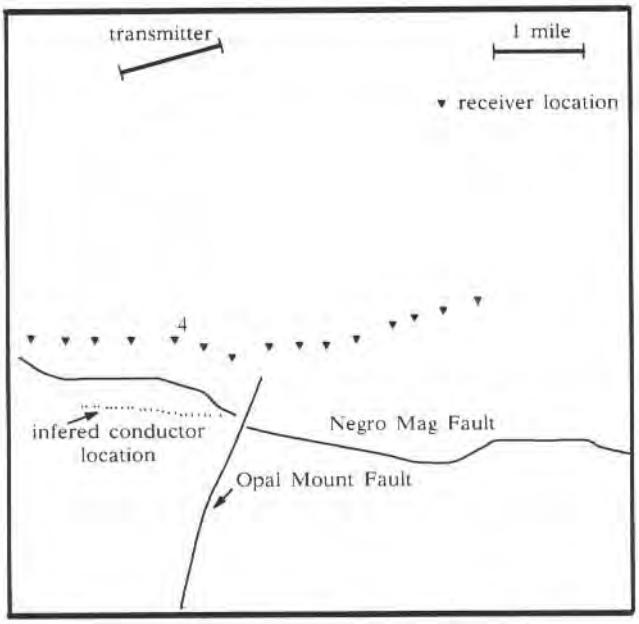

Fig.4.20: Station locations, faults and location of the modelled conductor for the Milford LOTEM survey (after Stoyer and Damron, 1986). Sounding 4 exhibiting a late time reversal is shown as example.

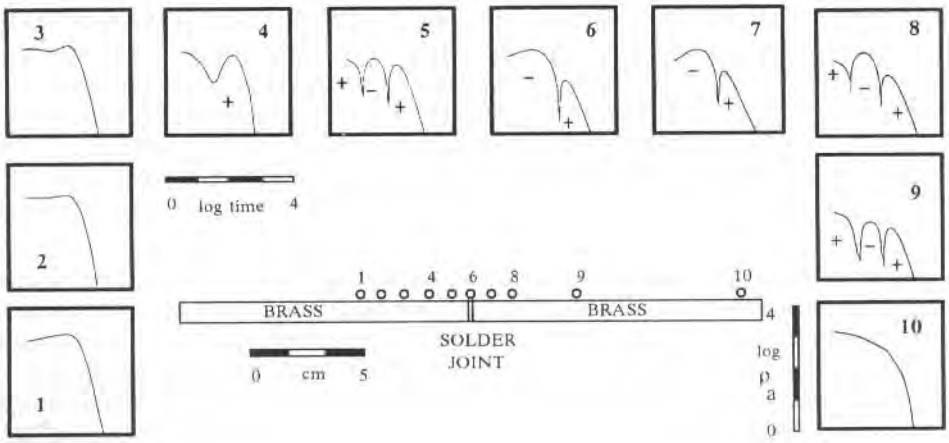

Fig.4.21: Simulation of a fault zone using an analog modeling experiment. The resulting shapes of the signal are used to classify the distorted responses (Stoyer and Damron, 1986). The station numbers are used as classification reference.

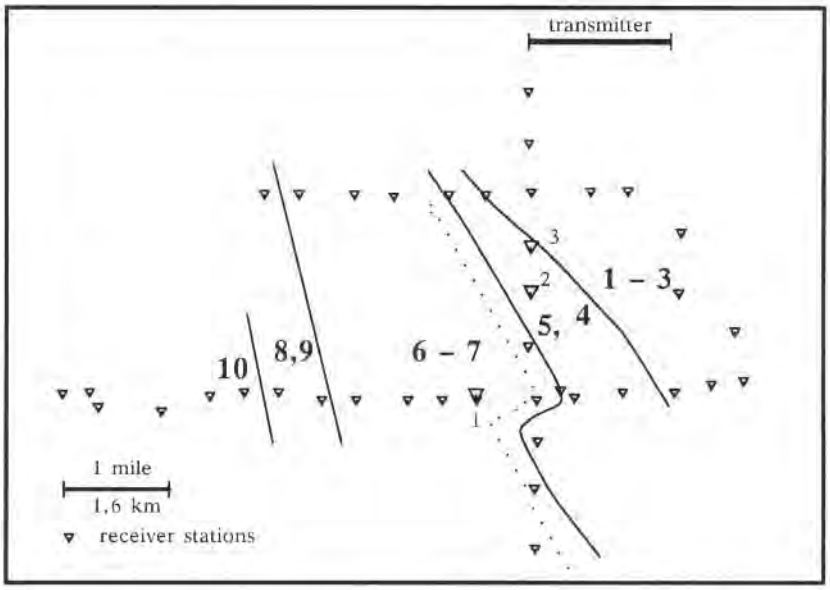

Fig.4.22: Interpreted *fault zone map* using the classification (bold numbers) for the distorted transients from figure 4.21 (after Stoyer and Damron, 1986). The large numbers refer to the curves shown in figure 4.18. The dotted line shows Stoyer and Damron's 1986 interpretation of the location of the fault.

and disappear more slowly (curves 6 to 10). The effect is expected to be stronger in the analog model, since the induction currents are more confined within the plate. Using the classification from the analog modeling results, part of the Milford data was interpreted yielding the interpretation shown in figure 4.22.

The analog modeling classification allowed the definition of possible fault zones. Resulting from this the location of the western boundary fault was inferred. There was also some geologic evidence for the existence of such a north–northwest trend. This geology is also numerically modeled and the results are shown below.

Stephan (1989) used the same approach and Damron's analog modeling results to classify his data from a survey in North–West Germany (Haltern). In parts of the survey area distorted transients were observed (see figure 4.23). Only in the north–eastern corner of the survey area could the reversals be attributed to geological structure. In other parts of the survey area the reversals were most likely caused by cultural noise (railroad tracks, pipelines etc.). The two sample transients displayed in the figure show different characters. The left transient has first a positive spike followed by a small narrow reversal. The right transient starts with a strong narrow reversal directly after the start of the signal. Using Damron's classification in figure 4.21 a possible fault map was prepared and is displayed in figure 4.24.

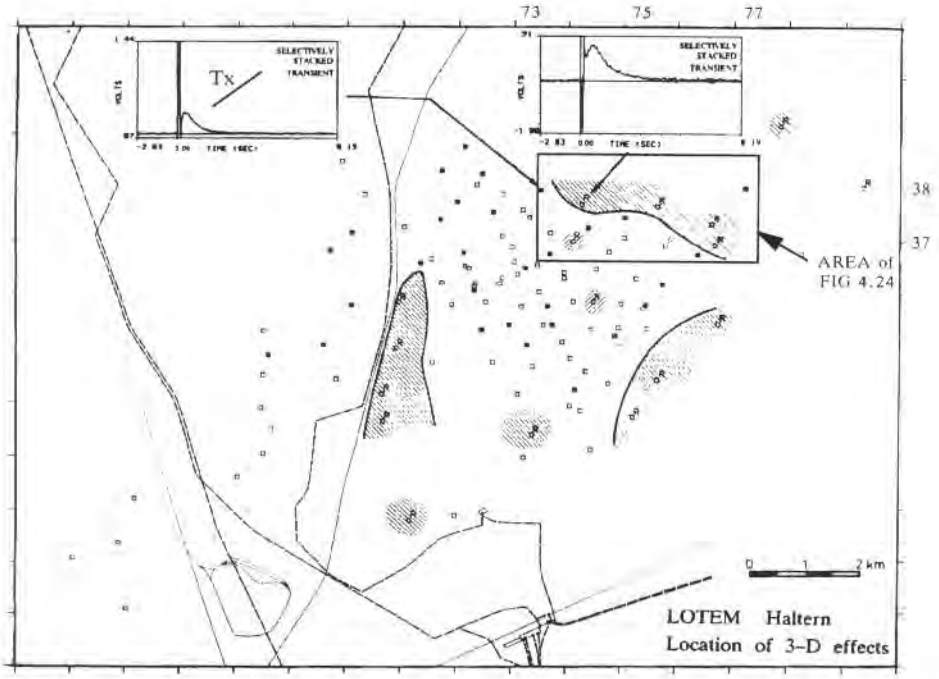

Fig.4.23: Survey map showing the location of distorted data (shaded areas). The shaded area in the north-eastern part exhibits reversals, two examples of which are shown in the figure (after Stephan, 1989). The dashed lines make the railroad and power lines.

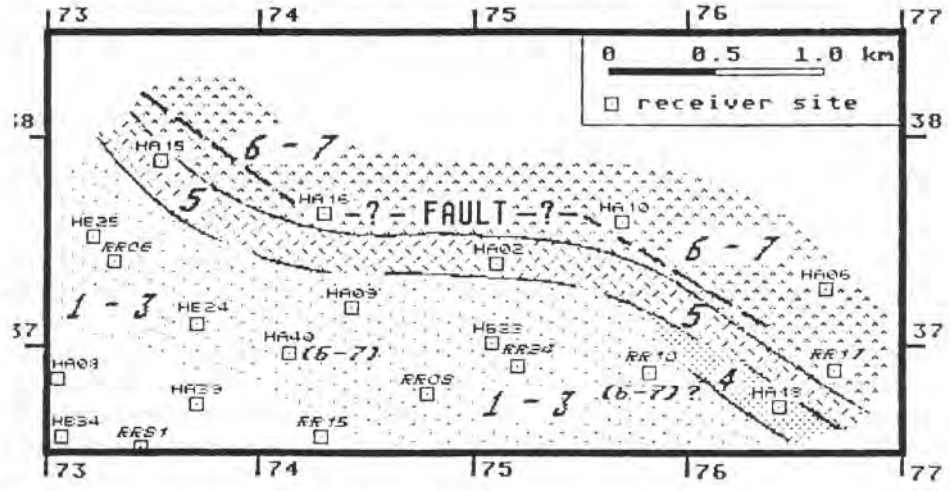

Fig.4.24: Possible fault maps for the Haltern Survey area using Damron's classification for distorted signals from figure 4.21 (after Stephan, 1989).

Using this kind of qualitative approach in combination with the field data allows an easy first classification of the distorted field transients. The next step is the integration of more elaborate modeling programs in the interpretation of real field data.

Numerical Simulation of Reversals

The numerical modeling of reversals is not an easy task, since *a priori* knowledge of the model structure is required. In this section two different numerical modeling approaches will be discussed. The first approach uses a laterally inhomogeneous conductive plate model to simulate the reversal (Weidelt, pers. comm.; Vasseur and Weidelt, 1977). The second approach uses the integral equation approach to calculate the 3-D response of an anomaly (Newman, 1989).

In the past, it was assumed that a reversal was caused by a conductive resistivity anomaly close to the receiver. This assumption was mainly based upon field experience and current channeling concepts. The conductive anomaly can be looked upon as a single conductor. The induction currents in this conductor remain strong for a long time and depending on what side of the conductor one places the receiver, the signal is positive or negative. Figures 4.25 and 4.26 show an example for a thin conductive plate model simulating such reversals (Weidelt, pers. comm.). The model is reduced to a thin plate with a conductance of 100 S located 100 m below the surface. Thickness and resistivity of the plate itself remain undetermined. The host rock has a resistivity of 10 Ωm. The resistivity values were selected from a real case history in Germany (see figure 4.24) simulating a resistive body. The offset between transmitter and receiver is 8 km. Figure 4.25 shows the time derivative of the vertical magnetic field for the receiver location marked in the upper part of the diagram. Reversals can be observed for the three stations on the far edge of the conductor and for three of the stations behind the conductor. The dashed lines on the graphs indicate the response for the earth without the conductive anomaly. The induction currents flow in the center of the plate causing on one side a positive and on the other a negative signal. The signal due to the anomalous conductor prevails with increasing distance from the transmitter. The anomalous response then adds to the normal response and depending upon its strength, reversals appear at different locations around the anomalous body.

The next model in figure 4.26 describes a more complicated field situation (Weidelt, pers.comm.). Now the conductive plate separates a 20 Ωm half-space from a surficial 12 Ωm layer. Part of the plate has a conductance of 10 S and the rest of 150 S. The layer above the plate has a resistivity of 12 Ωm and the one below of 20 Ωm. The corners of the conductivity anomaly are aligned with the equator of the dipole transmitter. In the plan view the conductivity anomaly is 3 km on the side and between 7 to 10 km away from the transmitter. The resulting time derivatives for the receiver stations are shown below. The response without anomalous zone is marked by the dashed line and differs strongly from the lower stations of the array. The station in the centre of the conductivity anomaly shows very little deviation between one- and three-dimensional curves. Again reversals occur only near the edge of the conductivity

anomaly. Again the specific occurrence of a reversal seems to be directly related to the strength of anomalous and normal fields with respect to the receiver position.

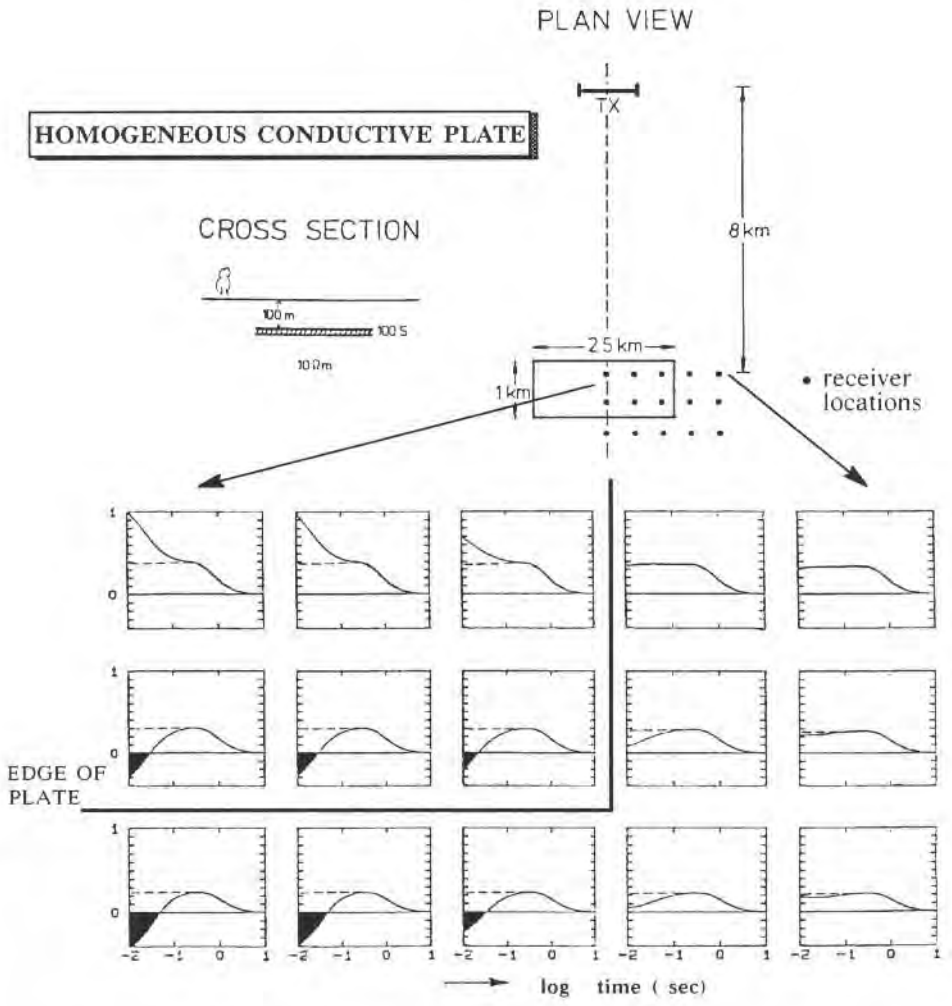

Fig.4.25: Field array and model for the conductive plate program simulating a sedimentary environment and the synthetic transients (semi–logarithmic axes) at the respective receiver sites. The conductive plate is laterally homogeneous (Weidelt, pers. comm.). The negative signals are displayed by area fill.

The second type of example uses Newman's 3–D (Newman, 1989) program to simulate a difficult field situation. The basic model and results are displayed in figure 4.27.

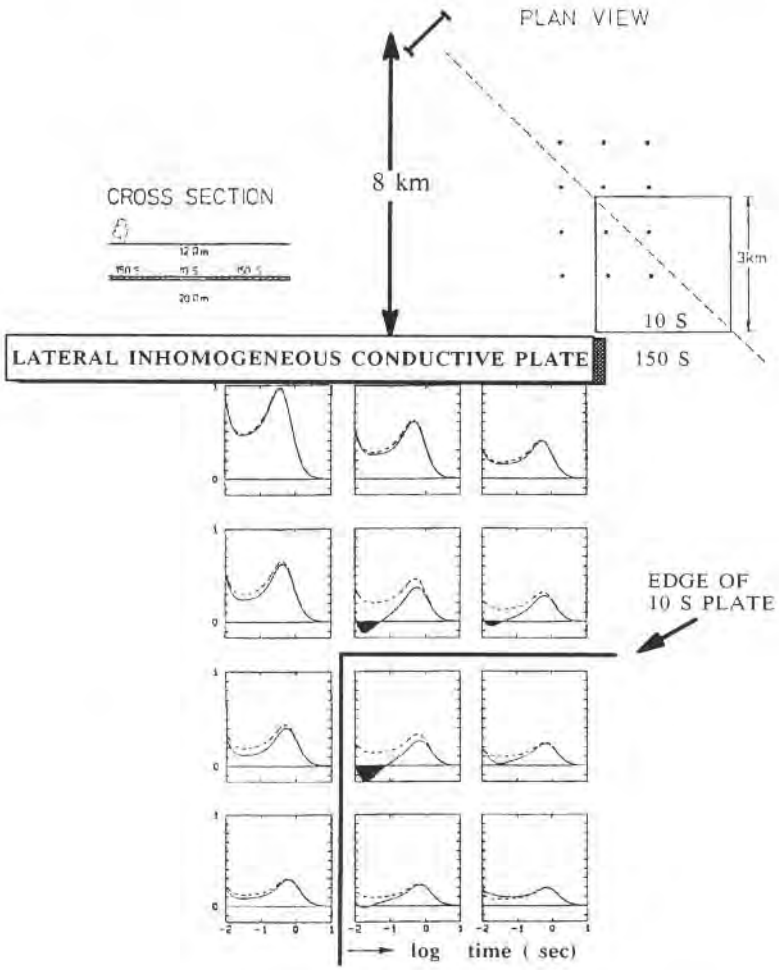

Fig.4.26: Geometric setup for the conductive plate program with lateral inhomogeneities. The model parameters simulate a sedimentary environment. The resulting synthetic transients (semi-logarithmic axes) are shown at the bottom.

This particular model simulates LOTEM measurements carried out in a crystaline environment with very high resistivities. The synthetic 3-D data (squares) are compared with a 1-D curve (solid line). The 1-D curve is the curve without the conductive anomaly (early time reversal). It can clearly be seen that the 3-D curve deviates very strongly from the 1-D curve until rather late times. On the right are the resistivity transforms of a field data set displayed which exhibits similar behavior. The difference in the zero crossing of the reversal is attributed to different scaling between the numerical model and the real geology under the receiver location where the data set

was acquired. The difference to the model of figure 4.26 is that the reversal was obtained with the conductive body between transmitter and receiver, whereas in the previous figure a resistive body beyond the receiver causes the anomaly.

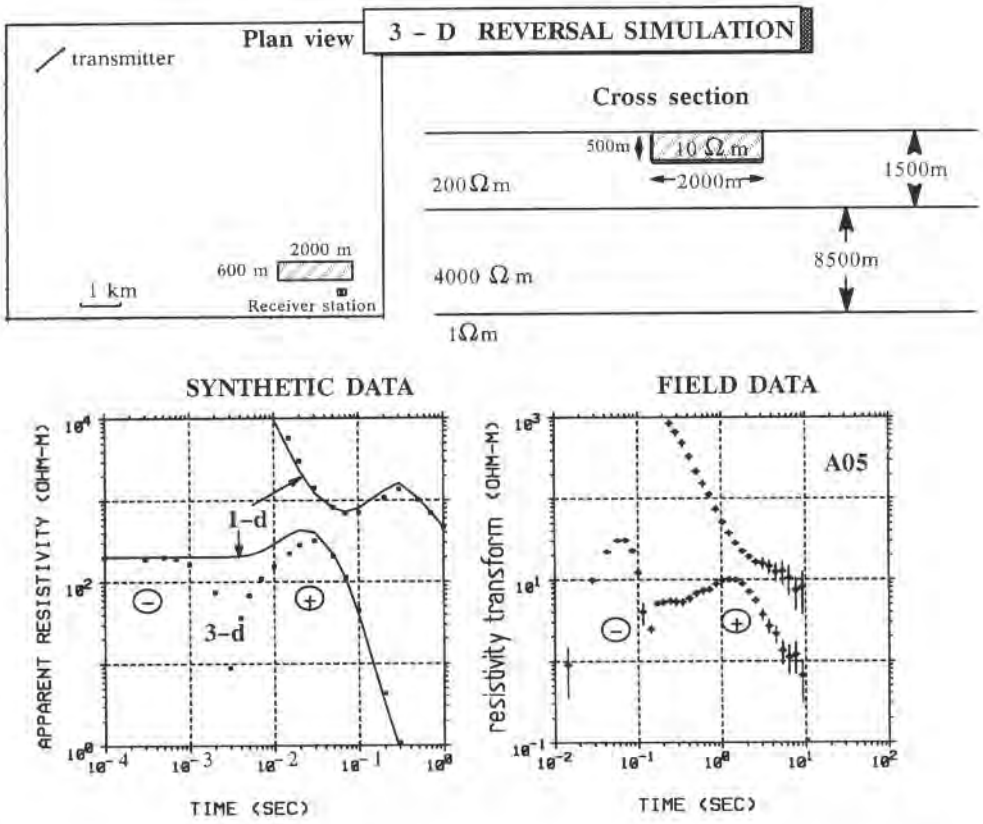

Fig.4.27: The three-dimensional response of a conductor near the receiver is calculated using the integral equation method. The top shows the section and plan view of the earth model. The data set on the bottom left shows the synthetic data for the 3-D model in comparison with the respective one-dimensional curve. On the bottom right a real field data set exhibiting the same characteristics is shown. The different location in time of the notch in both diagrams is caused by the model scaling and the fact that the detailed resistivity structure underneath the three-dimensional measurements is not known.

In order to evaluate the position of the reversals with respect to the location of the body further, Newman (1989) calculated the 3-D response for a profile across a conductive body. His results are displayed in figure 4.28. Two reversals can be seen in receiver location 3 and 5. The signals are distorted from receiver location 3 to 6. At site 3 the signal exhibits a sharp notch which is not yet a reversal. This is an indicator that we are approaching an anomalous zone. Similar behavior was also shown in

figure 2.19 where synthetic data of a 3–D structure was imaged. The location of the reversal behind the conductive body clearly indicate that the reversals occur near the conductivity anomaly when the response of the anomaly is larger than the layered earth response.

The above examples have shown two different ways of explaining reversals using analog and numerical modeling. In particular, they have demonstrated that reversals can be caused on either side of the conductivity anomaly. Also, reversals can be caused by resistive faults. Thus, for each particular survey where such reversals occur one should carefully eliminate all impossible options and pinpoint the conductivity anomaly by getting as much field data as possible to narrow down. Only then can successful 3–D modeling be done.

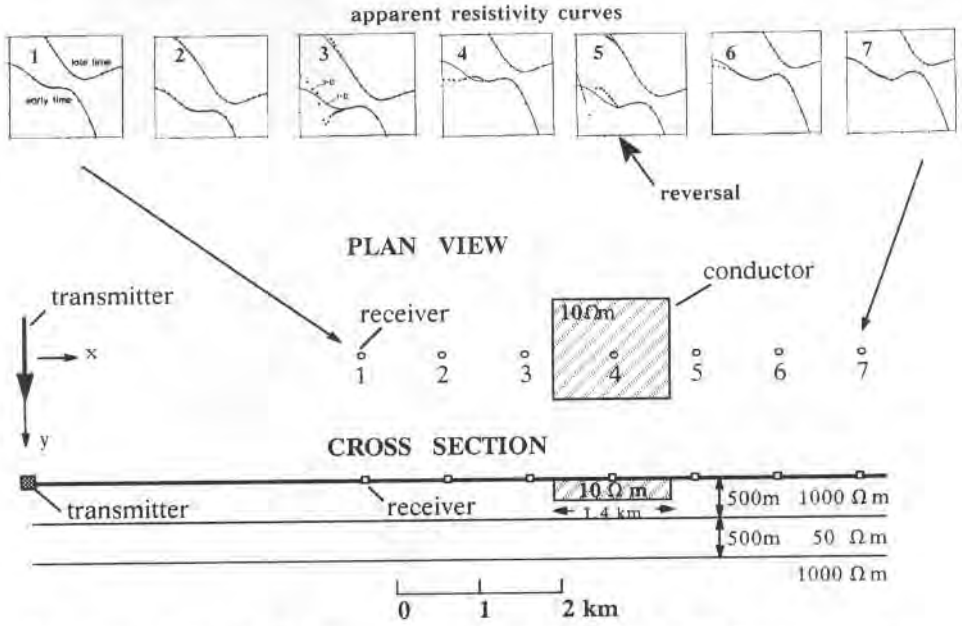

Fig.4.28: Model profile over a conductive body from 3–D modeling (after Newman, 1989).

With the above considerations, Kriegshäuser (1991) calculated two numerical models for the data from the Milford area, Utah. Based on Stoyer and Damron's (1986) interpretation the Negro Mag fault zone was simulated by a two–dimensional structure. From the above modeling results the conductor was placed at a similar depth the authors interpreted. The axial conductor has a very high conductivity to obtain the sign reversal at approximately the same time. Figure 4.29 shows the model setup and a comparison of a selected field data set with the respective numerical modeling data. For the modeling the finite difference program by Druskin and Knishnerman (1988) was used. The shape and amplitudes of the modeled and field data are very similar indicating that a very realistic model was selected. The remaining deviation between

the time of the sign reversal can be improved when changing the depth and conductivity of the axial conductor.

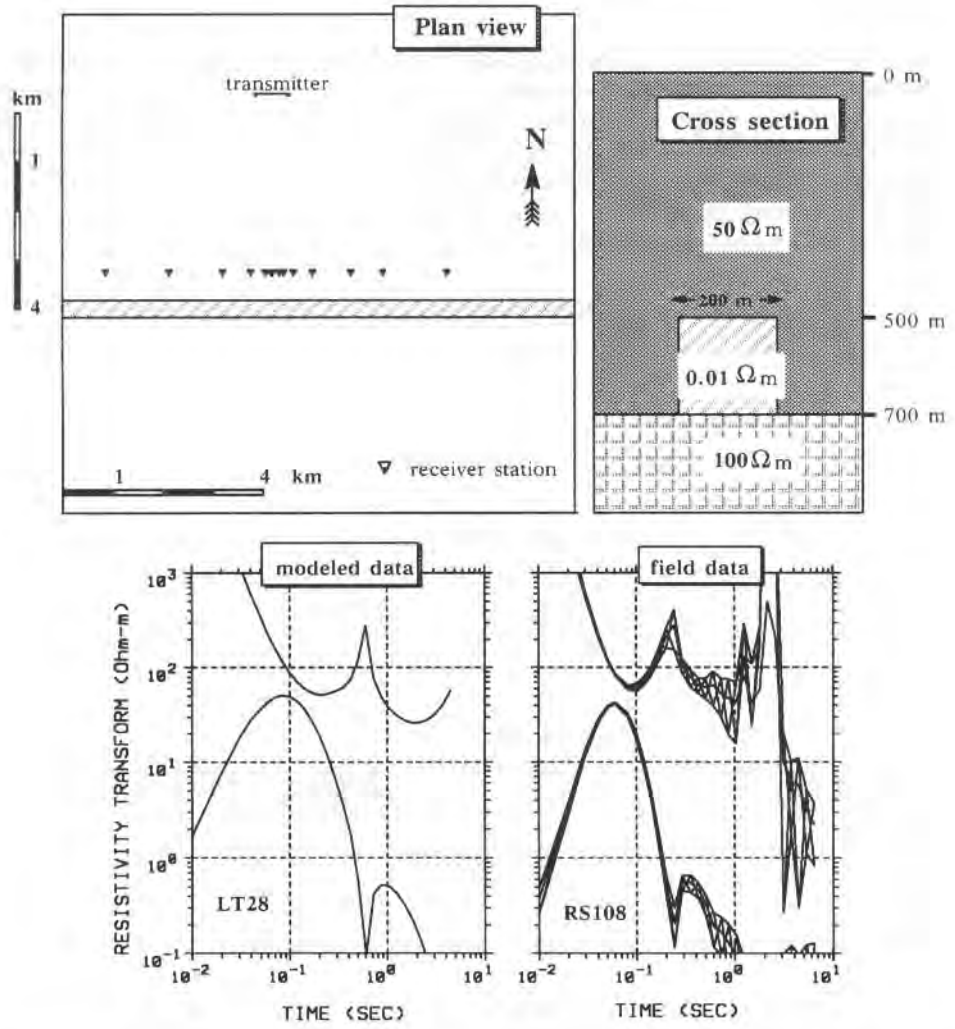

Fig. 4.29: Two-dimensional model setup for the axial conductor model of the Milford area, Utah. At the bottom of the figure a comparison between the synthetic and field data is shown. Both data sets are displayed as resistivity transforms. (after Kriegshäuser, 1991).

Another more detailed example is also from the Milford area but from the part of the survey which could previously only be interpreted with analog models. A three-dimensional model was constructed based on the one-dimensional interpretation of all data in the area with a resistive dike superimposed on it. The depth values for the 1-D

background model were selected from one-dimensional interpretation and the depth to the top of the dike and its width from the numerous different model runs. Figure 4.30 shows the survey plan with the dike outlined as well as a cross section of the model. On the left side of the figure characteristic transients are selected for the field data

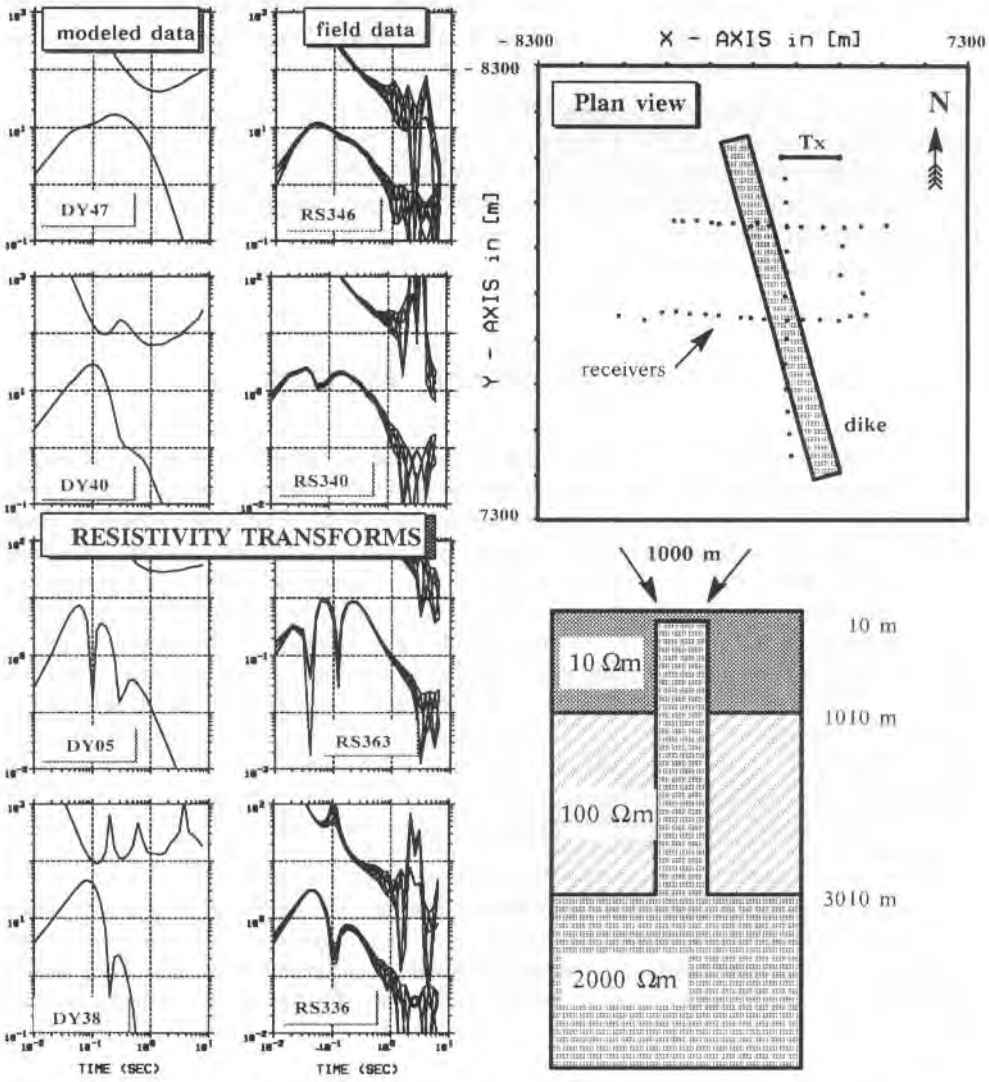

Fig. 4.30: Three-dimensional model setup (right) for part of the Milford survey. On the left the resistivity transform are shown for the modeled and field data.

and for the calculated data sets. The early time depression (top frames), the double reversal (third row of frames) and the intermediate time reversal match very nicely. The early time depression shown in the second row of frames is clearly exhibited by the field data but not so clearly by the modeled data. In fact, the modeled data shows the depression at significant later times. Although this appear to be a discrepancy, it is not so strong because the time window considered is still strongly effected by the system response. Only slight deviation it it, can cause the reversal to change its characteristics in this time range.

At this stage, it should be mentioned that it takes a long time and many different models before one can achieve a match between a 3-D model response and field data as shown above. When carrying out the 3-D modeling, the first task is to separate very near surface pipeline effects from deeper structural ones. this is usually done by looking at the strength of the reversals on a map. Also, the distribution of them and the initial polarity allow the interpreter to carry out this selection very effectively.

THREE-DIMENSIONAL MODELING

In order to interpret LOTEM data in three dimensions, one must have the necessary three-dimensional forward calculations on hand. Here, three techniques are being considered: the integral equation method, thin-sheet and finite difference. Several different researches have developed theory and routines for the integral equation method. Hohman (1971), Dey (1972) started with two dimensions and the extension to three dimensions was done by Raiche (1974), Hohmann (1975), and Weidelt (1975). The advantage of the integral equation method is the splitting of the electromagnetic fields in the response of the anomalous body and the surrounding medium. This reduces the size of the grid for the earth model. Wannamaker et al (1984) extended the algorithm to many layers. San Filipo and Hohman (1975) solved the integral equation for an anomalous body in a half-space directly in the time domain. Newman et al (1986) used Wannamaker's solution and transformed it via fast digital filters to the time domain. This is the algorithm which was used for the simulation of transmitter overprints.

The other approach uses the finite element method, but the problems for three dimensions for transient electromagnetics have not completely been solved. Kuth (Kuth, 1987; Kuth and Neubauer, 1988) developed an algorithm to calculate the three-dimensional response of an almost arbitrary earth for the frequency domain and an induction log tool.

Presently, the most flexible approach is using a finite difference scheme and the spectral Lanczos decomposition method (SLDM). The method was derived by Druskin and Knizhnerman (1988) and applied to real data for the first time by Hördt et al (1992). It can simulate very complex geology and calculate the 3-D response within a reasonable amount of computer time.

The first three-dimensional modeling for grounded wire TEM was done by Gunderson et al (1986). Their results gave the first insight into the 3-D current flows around a grounded wire. In all of their models the receiver was located less than four times the dipole length away from the transmitter and thus does not quite represent the LOTEM method. The first LOTEM modeling was done by Newman (1989). However, both above papers use resistivity contrasts which are not representative for exploration in sedimentary environment. For the derivation of the 3-D theory the reader is referred to several articles in Nabighian (1988). Here two practical examples of 3-D modeling are shown: The first example considers the effects of transmitter overprints, which are extremely common when carrying out field surveys. The second example compares the thin-sheet modeling program, the integral equation program and the SLDM finite difference program to simulate reversals, which occur frequently in the field.

Simulations of Transmitter Overprints

When carrying out field measurements, one usually looks for a transmitter site which allows the best electrical coupling of electrodes. Often, the transmitter is setup in a more conductive area or on a conductive patch. This will cause the signals to be slightly distorted. Routinely, the calibration factor (see chapter 3) is applied to the data to correct for this type of distortion. Here, this effect is investigated using 3-D numerical modeling.

Three-dimensional modeling can be used to simulate the influence of near surface inhomogeneities. In the following example the effect of field situations is demonstrated when the transmitter is located on top of a conductive body. Figure 4.31 (top) shows a plan view and a cross section for a simple 3-D model. The anomalous conductor has a resistivity of 10 Ωm and is embedded in a 300 Ωm half-space. The effect of the conductive body can be seen in the curves on the right side of the figure near the actual surface location. The comparison of site one and two shows that the effect does not strongly depend on the receiver position. At the bottom of the figure the section view is displayed. The situation modeled here is typical for German conditions such as encountered in the Black Forest area. The transmitter is usually deployed in the valleys with conductive valley fill while the surrounding is highly resistive. The conductor causes a downwards shift in the early time apparent resistivity curve and an upward shift at late times. As mentioned earlier in the discussion on the calibration factor, this shift can be corrected and layered earth models can be obtained.

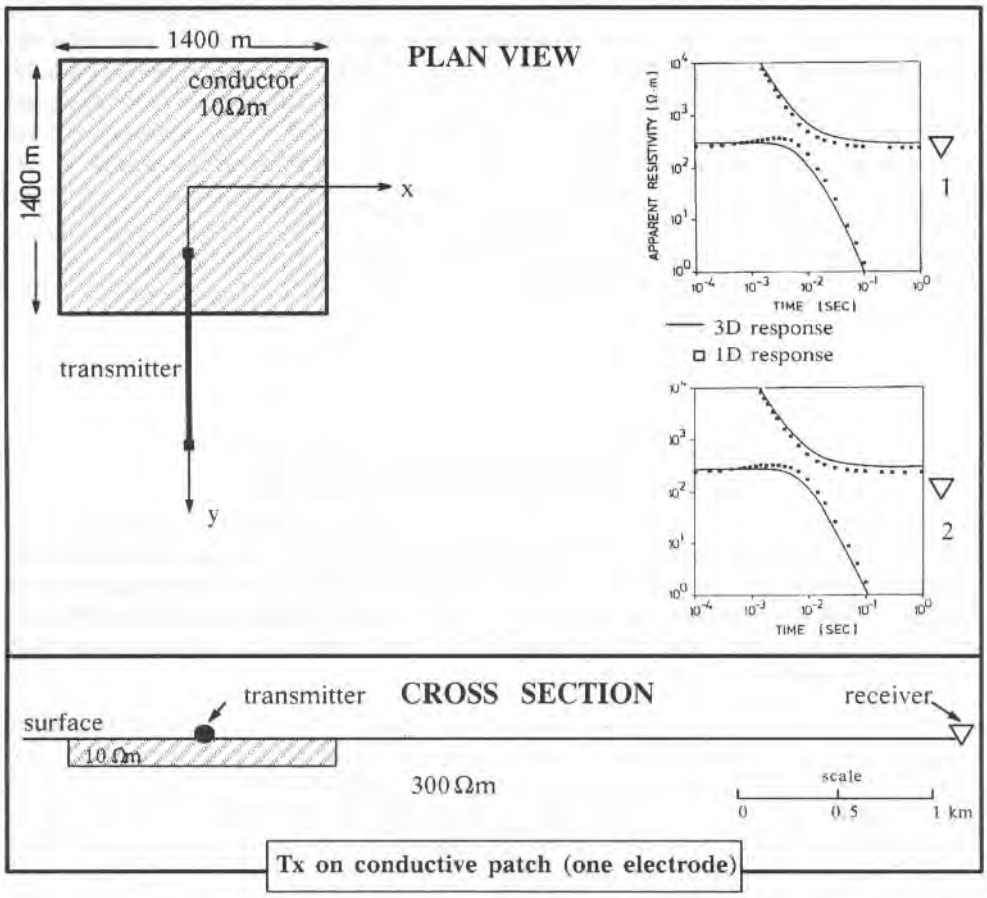

Fig.4.31: Plan view and cross section of the 3-D model to test the effect of conductive bodies underneath one electrode of the transmitter. For two stations the 3-D response (squares) and the 1-D response (solid lines) is shown on the right (after Newman, 1989).

Newman (1989) describes the results of interpreting the above model as yielding a biased layered earth model. Figure 4.32 shows the results of inverting the data from the 3-D model using a 1-D inversion algorithm. The inversion contained an additional parameter, the calibration factor, which is multiplied with the curve and thus shifts the curves vertically. The calibration factor was left floating during the inversion. The 3-D response is presented as data points in this figure. The solid lines through the early and late time curves are the synthetic curves for the inversion results. On the right side of the figure, the inversion models are shown in comparison with the true earth. The dashed line is the true earth model. Except for the upper part of the section

where an additional layer was introduced the resulting resistivity matches the true model. The data fit is quite acceptable. When using real field data, the model will in most instances be biased in the upper part of the section due to the effect of the system response. One thus needs a calibration well or additional information to make sure the interpretation is correct.

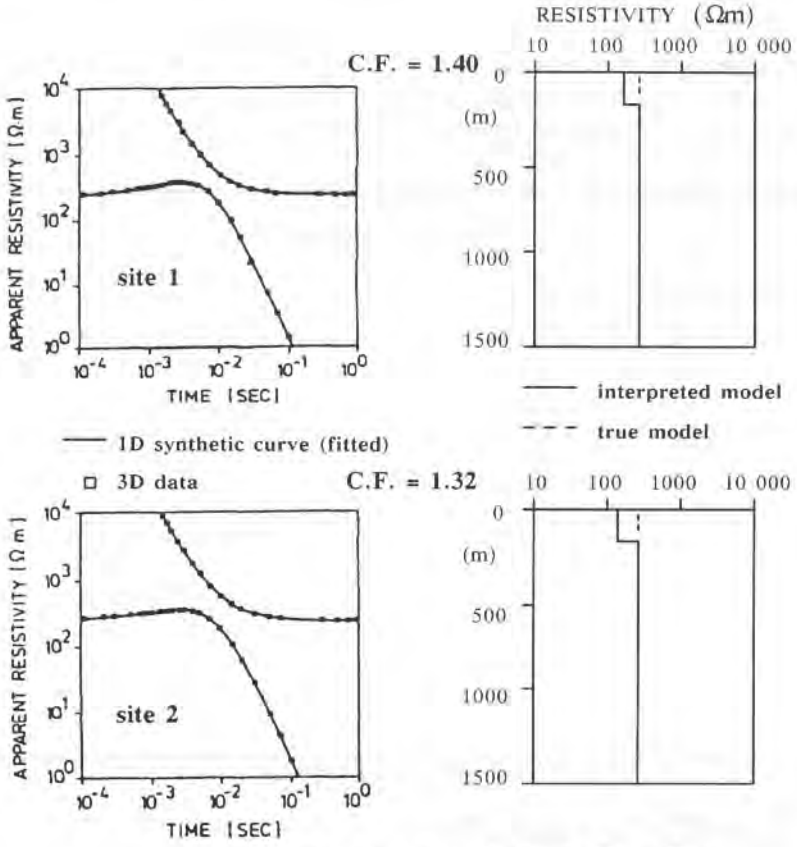

Fig.4.32: Interpretation results for the 3–D data of figure 4.31 using a 1–D inversion program (after Newman, 1989).

The system response must be considered in the interpretation because it masks the upper part of the section. In this case, when assuming that the model is typical for the Black Forest area (compare chapter 9), one would consider the following: In the Black Forest area, one is forced to use 16 2/3 Hz analog notch filters to obtain a useful signal. This restricts the reliable frequency content of the signal to below 10 Hz. One can use the diffusion depth $d = (2t\rho/\mu_0)^{1/2}$ (Spies, 1989) as a rough estimate for the depth when reliable data was acquired. For this case using a resistivity of 300 Ωm and

earliest time 0.1 sec (equivalent to 10 Hz), one obtains $d = (2 \cdot 0.1 \cdot 300 \cdot 107/4\pi)^{1/2} = 6900$ m. If the resistivity is to be slightly lower (200 Ωm) and the analog filters to effect the data from only 13 Hz onwards, this depth would be $d = 4900$ m. Since the diffusion depth represents the extreme case and usually the deconvolution removes some of the filter effects, one can assume for practical purposes that reliable information is obtained starting at half of the diffusion depth.

Very rarely, one finds a field situation where the upper crust is only resistive. Often the upper kilometers include some sort of conductive layers. Thus, one must consider the above effect using a horizontally layered earth model. Figure 4.33 shows the geometric setup and 3-D response for a layered earth host with an embedded conductor

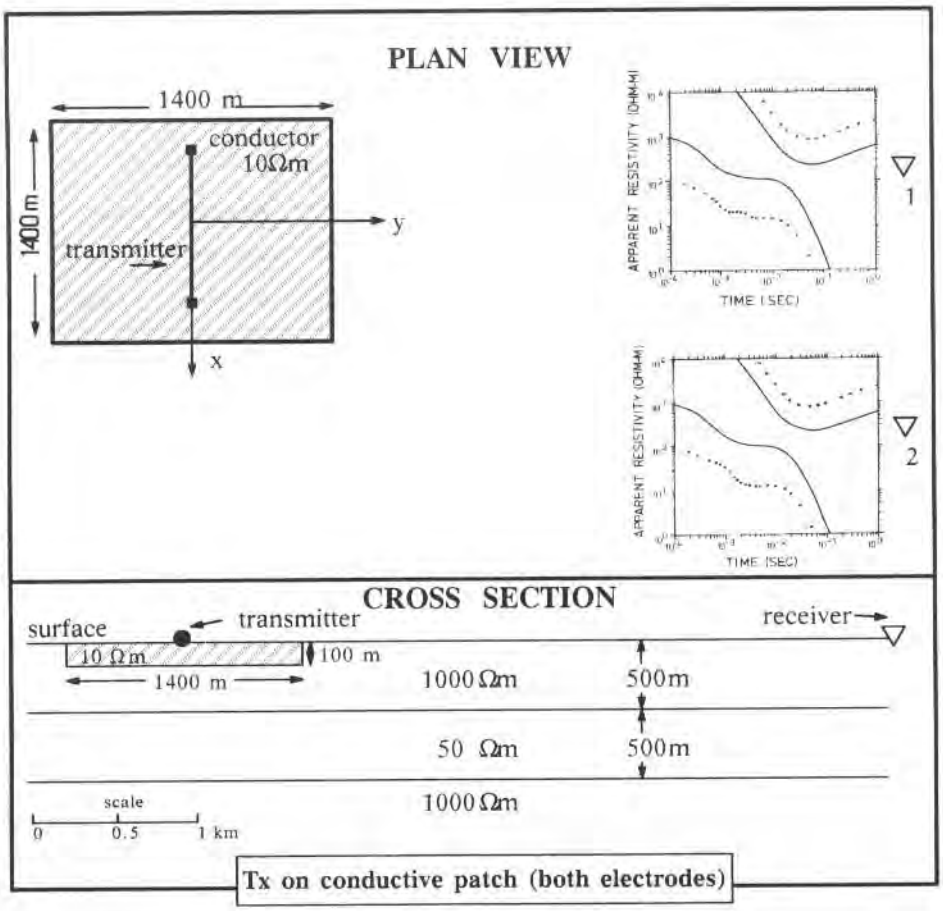

Fig.4.33: Geometric setup and calculated data for a conductor embedded in a layered earth with the transmitter located on top of the conductive patch (after Newman, 1989).

when both electrodes are located on a conductive plate. This is a very typical situation since one is always looking for the most conductive place to plant the transmitter. For both receiver locations the data is essentially parallel shifted at early and late times. When inverting the 3-D data with a 1-D inversion program (figure 4.34), an additional near surface layer is required for the interpretation. Also, the depth to the conductor is slightly wrong; its resistivity, however, is correct. Since the floating calibration factor in the inversion program has forced the data to be matched by a model one must be extremely careful when interpreting any part of the section below the conductor.

There are still some serious limits with 3-D modeling, since the integral equation method can only be used for confined bodies. This has little practical value for oil exploration since in most instances layered quarter-spaces are more important. Here one can envisage more use of layered quarter-spaces and a 2.5-D (two-dimensional earth and three-dimensional transmitter) model seems more appropriate. This is the reason why the application of a finite difference program using the spectral Lanczos decomposition method (SLDM) (Druskin and Knizhnerman, 1988) was considered for more complex structures.

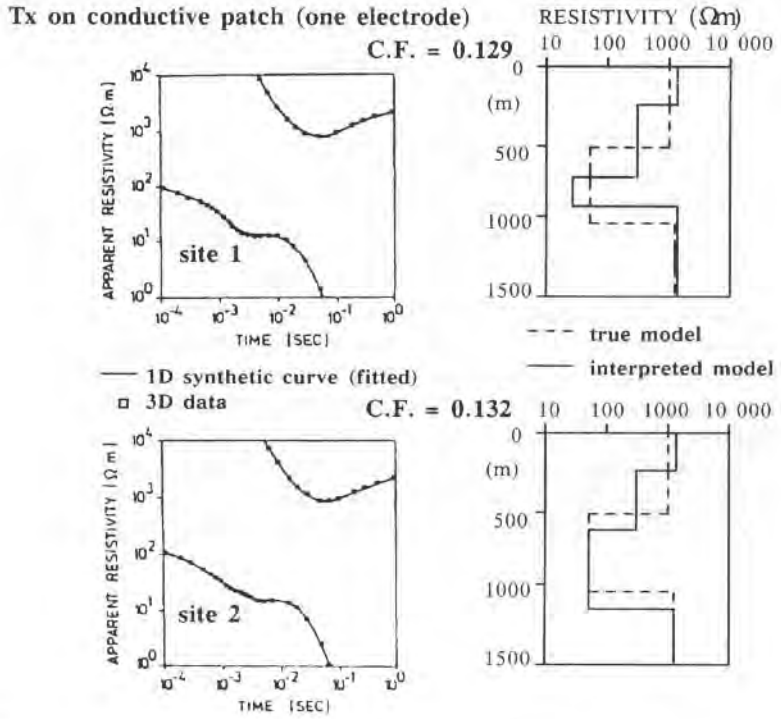

Fig.4.34: Interpretation results for the 3-D data of figure 4.33 using a 1-D inversion program (after Newman, 1989).

Comparison of Different 3–D Modeling Programs

In this section different 3–D programs are compared using a similar field situation as described in the chapter about reversals. The first program is a so called "thin–sheet" modeling routine. It calculates the transient response of an infinitesimally thin horizontal sheet, which is embedded in a layered half–space. The conductance, the product of thickness and conductivity, is finite. The algorithm is based on an integral equation (IE) technique (Vasseur and Weidelt, 1977). The main advantage of the program is its computational speed (about 5 min CPU time on a MicroVax computer for one earth model), allowing an inversion to obtain a rapid first order fit of the data. Since the resulting model is restricted to anomalous bodies of finite horizontal extent, which may not the be appropriate to the current problem, it is used to develop a starting model for more complex 3–D simulations.

The second program used is an integral equation program (Newman et al, 1986). It calculates the transient response of confined bodies in a layered half–space. There are theoretically no restrictions concerning the number and the shape of the bodies, but it can become very CPU time intensive for complicated models encountered in real exploration situations. This program forms the second step after the thin–sheet modeling for bodies of limited vertical and lateral extent. The goal is to approach a real geological model.

The third program (Druskin and Knizhnerman, 1988) is based on the spectral Lanczos decomposition method (SLDM) to solve the diffusion equation. This program is practically unlimited in terms of complexity using finite differences and allows the closest approximation of the real geology. The theory is described in Druskin and Knizhnerman (1988) and outlined in Hördt et al (1992).

The three programs are compared using the model shown in figure 4.35. A conductive body of 25 m thickness and 0.25 Ωm resistivity is embedded in a homogeneous half–space of 10 Ωm. The selection of the model is based on the above discussion on reversals. The thin–sheet modeling simulates the body with a conductance of 100 S. Synthetic data were calculated at three different receiver sites, marked on the right in figure 4.35. The transmitter is located 8 km away from the body with the dipole being parallel to the strike. This type of model is of those giving sign reversals. In the field, these sign reversals are a clear indicator of a three–dimensional structure.

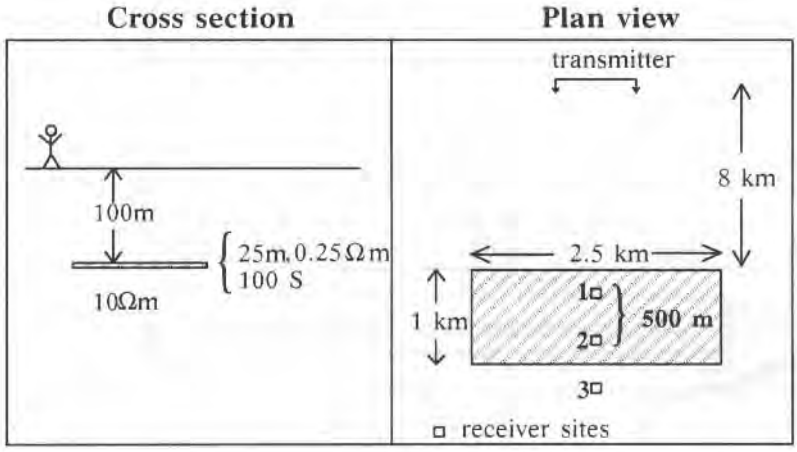

Fig. 4.35 The 3–D model used to compare the forward modeling routines. For the thin–sheet program the conductive body is infinitesimally thin, with a conductance of 100 S. For the two other programs (integral equation and finite difference, SLDM) the body is 25 m thick, with a resistivity of 0.25 Ωm (after Hördt et al, 1992).

The modeling results for the different programs are compared in figure 4.36. In the upper row the thin–sheet modeling is compared with the integral equation program. For all three receiver sites the two curves match well at late times (greater than 500 ms). For site 1 the curves diverge only at very early times. The greatest difference occurs for site 2. The deviations may be caused by the slightly different model, because the thin–sheet program uses an infinitesimally thin body, whereas the body is 25 m thick for the integral equation program. Considering this, the discrepancies may be regarded as small; and the general characteristics are similar between the models.

The second row shows the comparison of the SLDM results with the integral equation program. Again, for the late times the match is very good. A deviation of the curve occurs for early times and is the greatest for site 2. In this case, we also must consider that the earth model is difficult for the SLDM algorithm because the anomalous zone is confined to a small area and causes high field gradients. For the integral equation program the model is almost ideal. As for the upper row the difference can be considered negligible, confirming that all three programs give comparable results.

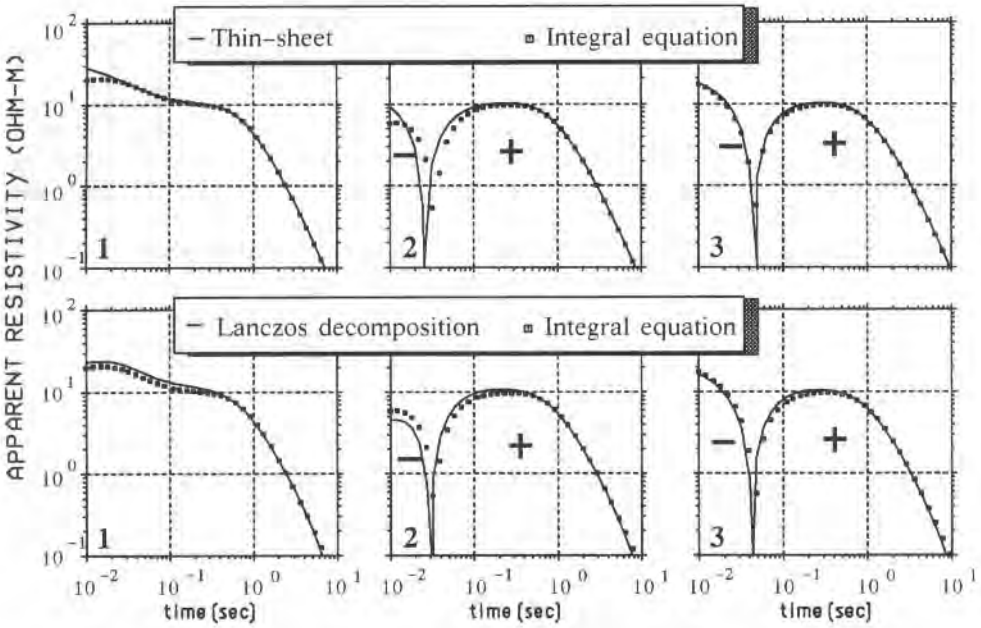

Fig. 4.36: Comparison of calculated data for the configuration of figure 4.35. Upper row: The solid line is the result usingthin–sheet modeling. The squares are the results using the integral equation (IE) method. Lower row: The solid line is the result using the spectral Lanczos decomposition method (SLDM). The squares are the results using the IE method (after Hördt et al, 1992).

SUMMARY CHAPTER 4

The standard interpretation of deep transient electromagnetic soundings is done using one–dimensional inversion algorithms. The interpretation is "trying" to derive from the measured data the most likely subsurface resistivity as a function of depth. One–dimensional inversion can be used in several different ways to obtain a more objective estimate of the subsurface resistivity: individual inversion at each site; joint inversion of several components or different electromagnetic measurements; automatic inversion along a profile; or inversion of the data yielding a smooth resistivity versus depth function (Occam inversion). When applying all these different inversion techniques one is still left with a small number of anomalous soundings which have to be interpreted initially in a qualitative way until quantitative three–dimensional modeling can be done.

Most routinely inversion is applied to a single sounding at one station. To obtain estimates for the reliability of the inversion results, the statistics and its analysis are just as important as the inversion itself. In most real field situations in sedimentary

environment this type of inversion will already give sufficient information about the resistivity structure of the subsurface. Sometimes, this type of interpretation does not yield the information requested because of the sensitivity bias in the component (electric or magnetic field) selected for inversion.

To reduce the bias in the sensitivities of the individual electromagnetic field components, two different components can be inverted at the same time in a joint inversion. A joint inversion can also be done using one TEM component together with magnetotelluric data. Joining two different electromagnetic techniques has the advantage that each of them can compensate for the weaknesses of the other and in a joint inversion a more objective and realistic result is obtained.

One of the important parts in interpreting transient electromagnetic soundings is the time spent inverting similar data sets from scratch. Thus, one can use an inversion procedure which integrates the *a priori* information of the previous station for the next station. This inversion procedure is called profile inversion. There are several ways of choosing how this *a priori* information is being integrated and one should carefully apply it depending upon the problem of the specific target area. With this type of inversion extreme care should be taken, because one can also force the data to match the expectations of the interpreter.

In order to cross-check the interpretation results one is searching for a unique resistivity versus depth function. This type of unique result can be obtained using the Occam inversion. The Occam inversion is based on the assumption that the resistivity versus depth distribution is smooth. This works well in sedimentary environment with no abrupt resistivity changes in the subsurface. In those cases the Occam inversion which is very computer time intensive can be used to cross check the interpretation results.

When applying the different inversion techniques the interpreter sometimes faces the problem that specific transients behave abnormally and cannot be interpreted. One type of these abnormal transients is when the measured voltage crosses the reference level. These transients are called reversals. Due to the limitations of three-dimensional modeling it is very difficult to quantitatively interpret these reversals. Thus, one first tries to use the reversals to obtain a map of this three-dimensional geologic structure in the survey area. Once the interpreter understands the nature of the three-dimensional structure simple three-dimensional models can be calculated and a more quantitative estimate of the structure obtained. The different techniques for three-dimensional modeling include asymptotic formulations, reduction of the three-dimensional anomaly to a thin inhomogeneous conductive plate, and integral equation methods. All of the techniques yield interpretations of resistive fault zones or conductive patches between the transmitter and the receiver.

The selection of the appropriate 3-D modeling routine is very important. One should always evaluate different routines using characteristic effects in the field data. In this chapter, using the different routines gave comparable results for the interpretation of a characteristic reversal.

PROBLEMS CHAPTER 4

1. Explain the process of inversion.
2. What is the Jacobian and what does it mean?
3. Explain the difference between the *Marquardt–Levenberg* method and the gradient method.
4. Why does the inversion often use logarithmic parameters?
5. How do the transformed parameters relate to the original parameters?
6. Why do we use *joint inversion*?
7. How do you determine a correlation between model parameters?
8. What would you use *profile inversion* for?
9. In what geological environment should we not use the *Occam inversion* philosophy?
10. What would you do when you start observing reversals on a walkaway profile in the field?
11. How do we routinely compensate for transmitter overprints in the magnetic field signal?
12. Explain possible applications for the three 3–D programs discussed here.

KMS Technologies – KJT Enterprises Inc.
6420 Richmond Ave., Suite 610
Houston, Texas, 77057, USA
Tel: 713.532.8144

Please visit us
http://www.kmstechnologies.com